Eur. J. Mineral.
2002, **14**, 263-289

Neutron diffraction applied to geological texture and stress analysis

WOLFGANG SCHÄFER*
Mineralogisch-Petrologisches Institut, University of Bonn *in* Forschungszentrum Jülich, MIN/ZFR,
D-52425 Jülich, Germany

Abstract: Texture is defined as preferred crystallographic orientation in a polycrystalline aggregate. The main mechanisms of geological texture formation are crystallization, sedimentation, plastic deformation, recrystallization and metamorphism. Textures of geomaterials are fingerprints of the earth's history. The complexity of geological texture analysis results mainly from the overprinting of different textures on several mineral components during different orogenic periods. Quantitative texture analysis, *i.e.*, the calculation of a three-dimensional orientation distribution function of crystallites, is based on experimental pole figures which represent the orientation distributions of certain crystallographic directions and which can be obtained from X-ray or neutron-diffraction techniques.

Due to the high penetration capability of neutrons, large specimens can be investigated resulting in global volume textures rather than local surface textures from X-rays. Neutron-diffraction pole figures are characterized by high grain statistics even on coarse-grained material. Individual pole figures can also be obtained from reflection-rich diffraction patterns of multiphase rocks and low-symmetry mineral constituents by using position-sensitive detectors and by pattern decomposition by means of profile-fitting methods. Neutron texture diffractometers are operated in the constant-wavelength mode at steady-state sources and using time-of-flight techniques at pulsed sources. Different experimental set-ups are discussed.

Results of neutron-diffraction texture analyses on monomineralic and polymineralic rocks are presented, *e.g.*, on calcite, quartzite, plagioclase, pyrrhotite ores, granite, and orthopyroxene-sillimanite-granulite. The wide application spectrum of neutron texture analysis includes objects of the outer solar system as in the low-temperature texture study on ice and the non-destructive investigations on rare pieces of meteorites.

The application of neutron diffraction on strain measurements and residual stress analysis of geological material is discussed. Natural effects on rocks are orders of magnitude smaller than in technological material and drilling gives rise to stress relaxation. Experimental deformations can be observed during *in situ* measurements at various pressures and temperatures. Neutron strain diffractometers are described. Examples of recent results on the full strain/stress tensor in sandstone and on strain partitioning in polymineralic rocks are given.

Future prospects of new high-intensity neutron sources are promising in performing combined structure, texture and stress analysis. New instruments are under construction and software packages on the basis of full-pattern Rietveld refinements are available.

Key-words: texture, strain/stress, neutron diffraction, geological materials.

1. Introduction

The term texture is used as a synonym for preferred crystallographic orientation in a polycrystalline aggregate, as it has been used for a long time in metallurgy, and also in geology. Texture is one of the fundamental features of the total internal structure of a rock which, generally, is referred to by the term fabric. Apart from the texture, the fabric is characterized by the various minerals constituting the rock and by the microstructure comprising the shapes and sizes of grains, the spatial relations between them, and the substructures within the grains which may also be influenced by the occurrence of residual stress.

Rocks, as opposed to metals, show a great variety of textures and compositions, generally containing several phases with very different physical and chemical properties. Most rocks are brittle rather than ductile. Ionic and covalent bonding predominate in minerals, resulting in low-symmetry crystal structures and large unit cells. Many rock-forming minerals, *e.g.* silicates, are in the monoclinic and triclinic crystal systems whereas metals are in the high-symmetry cubic or hexagonal crystal systems.

Apart from these differences in the materials themselves, the major objectives of texture analysis are also different in material and earth sciences. While in material sciences the major emphasis is on the development and

*e-mail address: w.schaefer@fz-juelich.de

0935-1221/02/0014-0263 $ 12.15
DOI: 10.1127/0935-1221/2002/0014-0263

control of required preferred crystal orientations under well-defined experimental conditions of material processing in order to guarantee specific (anisotropic) macroscopic physical properties, the problem in geosciences is approached the opposite way and has many more implications. The geologist begins with the end product, the rock, as it occurs in nature, and attempts to reconstruct the processes by which the texture has been formed. The texture is a fingerprint of the earth's history and, simultaneously, informs on anisotropies of elastic, magnetic, and thermal properties of rocks constituting the crust and the upper mantle. Anisotropy needs to be taken into account in the interpretation of seismic data, development of geophysical models, and geophysical prospecting.

Geological texture and stress analysis is made difficult by the complexity and the slowness of natural processes over millions of years. The evolutionary history of texture formation often involves more than one orogenic period resulting in overprinting of several events widely separated in time. The main mechanisms of geological texture development are (1) crystallization, (2) sedimentation, (3) plastic deformation, (4) recrystallization and (5) metamorphism as reviewed by Skrotzki (1994).

(1) Crystallographic preferred orientation is already formed during crystallization. For many rock-forming minerals such as mica or feldspars crystal-growth rates are anisotropic and hence, crystals develop with unequal shapes which are directly related to crystallographic forms. Anisotropic growth may yield an alignment of the fastest growing direction parallel to the temperature gradient. The textures produced by anisotropically shaped crystals in a flowing magma have orthorhombic and monoclinic symmetry in pure and simple shear, with the longest and shortest crystal extension being aligned parallel and inclined to the shear direction, respectively.

(2) Similar to crystallization, axial symmetric preferred orientation is settled during sedimentation of anisotropically shaped crystals, *i.e.*, when being transported in a medium like air or water. Examples of these texture formations may be found in amphiboles, phyllosilicates, or clay minerals.

(3) Changes of crystallite orientations develop during plastic deformation by slip and/or twinning. During sufficient deformation depending on temperature and strain rate conditions, a crystal with one slip system will reorient itself into a position where the glide plane is normal to the maximum compression direction and the glide direction parallel to the extension direction. The assignment of special slip systems to the mineral constituents of a rock is a central task of texture analysis. Mechanical twinning is a deformation mode which is observed in many minerals and generally occurs at low temperatures and/or high strain rates (*e.g.*, in calcite). In general, mechanical twinning is restricted to a partial volume of the aggregate or even the crystallite. The importance of twinning lies in the large orientation changes which may lead to a change of the slip system and hence to a strengthening of certain texture components.

(4) Recrystallization occurs during static annealing of a deformed material under its melting temperature. Very small grains are nucleated and grow at the expense of the deformed material. The driving force for primary recrystallization is the elastic energy stored in the dislocations of the deformed material. The components of a recrystallization texture are already contained in the deformation texture. Static recrystallization, however, is of minor importance in geological rather than in metallurgical materials, as high-temperature annealing of rocks is very rare in nature. Under geological conditions, rocks deform plastically only at elevated temperatures and usually deformation is accompanied by dynamic recrystallization.

(5) Metamorphism is the mineralogical and often structural transformation of rocks in the solid state due to changes of physical and chemical conditions. Texture formation in metamorphic minerals is the result of different mechanisms. Examples of these transformations are *e.g.*, calcite to aragonite, pyroxene to amphibole, or the reduction of hematite to magnetite.

This short survey on geological texture formation and development may give an impression on the complexity of geological texture analysis which, in the past, was widely limited to a phenomenological approach. Nowadays, knowledge has reached a level that provides a quantitative framework of texture information. Progress of quantitative texture analysis in geosciences, obtained more recently, and first results of quantitative strain/stress analyses on rocks are based (1) on the improvements of the experimental techniques with special emphasis on diffraction methods and the use of neutrons, and (2) on the application of mathematical methods developed in material science to model three-dimensional orientation distributions and stress tensors on the basis of reliable diffraction data.

Quantitative texture analysis is aimed at: the determination of the orientation distribution of crystallites in the polycrystalline aggregate, the interpretation of this distribution in terms of the processes which lead to its formation, and the establishment of a relationship between orientation distribution and macroscopic properties. Particularly the following aims in earth sciences are envisaged, compare Bunge (1997): (1) Information about geological processes which have taken place millions of years ago. (2) Information about anisotropic properties in field samples and relationships to results of macroscopic physical measurements (*e.g.*, magnetization) and materials constants (*e.g.*, elasticity) for the interpretation of seismic data. (3) Conclusions from well-defined artificial deformations (*e.g.*, of ores) on natural textures. (4) Texture influence on technological properties of rocks used as building materials in industry and architecture (*e.g.*, marble, granite). (5) Plastic anisotropy of salts and flow behaviour of caverns in the salt deposits. Surveys on texture analysis with respect to geological materials may be found in Wenk (1985), Bunge *et al.* (1994), Kocks *et al.* (1998), and Leiss *et al.* (2000).

The orientation distribution of crystallites in a rock, as a consequence of the microscopic mechanisms and of the strain path, can be used to get some insight into the deformation history. This, however, is never unique as discussed by Wenk & Christie (1991) in a review paper on the interpretation of deformation textures in rocks. The polycrystal-

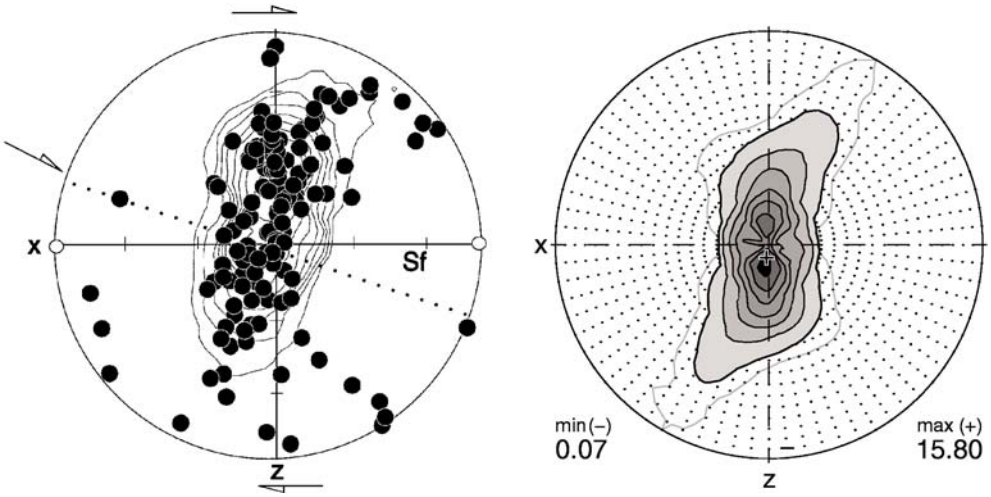

Fig. 1. Comparison of c-axis pole figures of a quartzite obtained from U-stage microscopy (left) and neutron diffraction (right), based on investigations of about one hundred and one million grains, respectively; Ghildiyal *et al.* (1999).

plasticity theory is very important for the understanding of preferred orientation patterns. A balance between stress equilibrium and strain compatibility is needed for modelling deformation and between nucleation and grain growth for modelling recrystallization. In this task close collaboration with material scientists is essential.

2. Texture analysis from experimental pole figures

The texture of a polycrystalline material is defined by the orientation-distribution (or density) function (ODF) of its crystallites. The ODF can be described by

$$f(g) = \frac{1}{V}\frac{dV}{dg} \qquad \text{with } g = [g_{ik}] \tag{1}$$

defined by the volume fraction of crystallites having an orientation g. The orientation g can be defined by a transformation matrix g_{ik} describing the orientation of the crystallites with reference to a coordinate system, the axes of which are defined by rolling and lineation or foliation when regarding metallic and geological materials, respectively.

The ODF cannot be measured directly without destruction of the specimen, it can only be reconstructed from two different kinds of measurements. One (traditional) method is the optical measurement of individual orientations of a representative set of crystallites using universal-stage microscopy. Much faster and more efficient than the painstaking optical work (Fig. 1) is the derivation of the ODF from experimental pole figures P_{hkl} which are obtained from electron (in particular electron-back-scattering), X-ray or neutron-diffraction techniques by measuring the orientation distributions of certain crystallographic directions [hkl].

$$P_{hkl}(y) = \frac{1}{2\pi}\int_{y\perp(hkl)} f(g)d\psi \quad \text{with } y = \{\alpha, \beta\} \tag{2}.$$

Pole figures represent pole density functions (PDF) of pole coordinates $\{\alpha, \beta\}$(compare Fig. 3). Since pole figures are two-dimensional projections of the three-dimensional ODF, this implies the problem of calculating the ODF from a finite number of experimental pole figures. This problem is called pole-figure inversion and has, generally, no unique solution.

Different mathematical procedures have been developed to calculate the ODF from experimental pole figures. Depending on the method, the calculated ODF is a continuous or a step function. A method which is widely and predominantly applied in texture analyses of high-symmetry materials, is the series-expansion or harmonic method developed by Bunge (1982) (see also Dahms & Bunge, 1989). According to the classic harmonic approach, an orientation-density function is expanded into its corresponding Fourier orthogonal series with respect to generalized spherical harmonics. Routine computer programs are available to perform these calculations. A different mathematical approach is the discretization method based on the maximum-entropy concept using a finite series expansion into indicator functions. This method was introduced into and adapted for the purpose of texture analysis also in view of applications in the geosciences by Schaeben (1988, 1994) with the program MENTEX. The so-called WIMV-method developed by Matthies (1979), which is rather common in geological texture analysis, is based on certain probability assumptions of f(g) which may then be further improved by iterative refinements (Wenk, 1985).

Contrary to the global description of texture in the total orientation space, texture may be described only for restricted ranges of the orientation space by a certain number of texture components. The application of the so-called component method developed by Helming & Eschner (1990) is realized by the program MULTEX written by Helming (1996). Each component, which may be described by, for instance, Gaussian peak distributions, is given by a preferred orientation g^c locally restricted in orientation space, a half width b^c characterizing the spread around g^c (Fig. 2) and an intensity I^c identical to the volume part of all crystallites belonging to that component. The ODF approximation by means of texture components is expressed by

$$f(g) = F + \Sigma\, I^c\, f^c(g) \tag{3}.$$

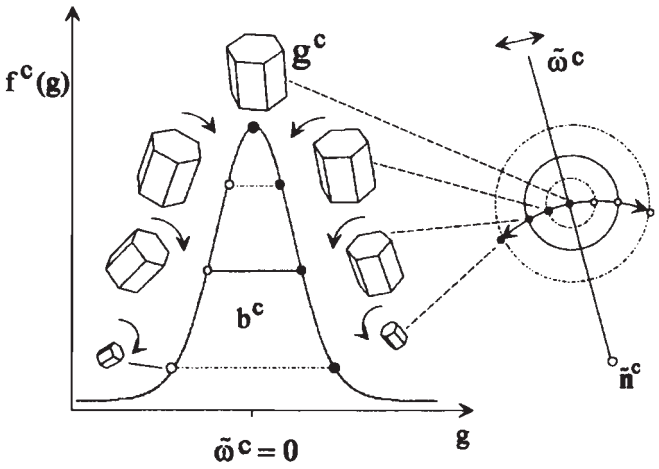

Fig. 2. Representation of a texture component with a maximum at a preferred orientation g^c by a Gaussian model function $f^c(g)$ decreasing with increasing deviation from $\omega^c = 0°$ by rotation about an axis $\tilde{n}^c$ perpendicular to the plane of drawing; Helming (1996).

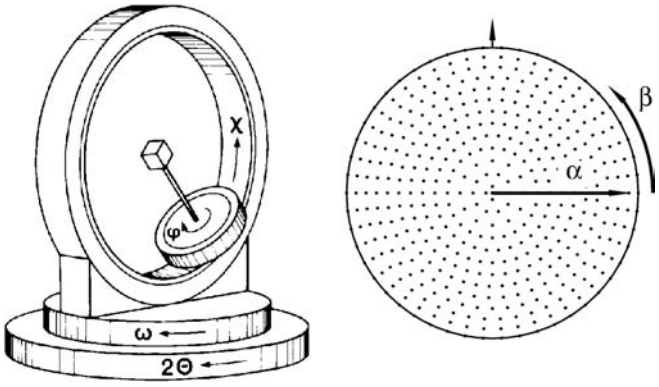

Fig. 3. Eulerian cradle with rotation axes φ, χ (left) and (α, β) pole-figure scanning grid (right); Höfler *et al.* (1988).

The quantity F gives the volume fraction of the randomly oriented crystallites, *i.e.*, not restricted in the orientation space. The component method, as the WIMV-method too, can be applied to composite experimental pole figures of multi-phase geological material of any crystallographic symmetry.

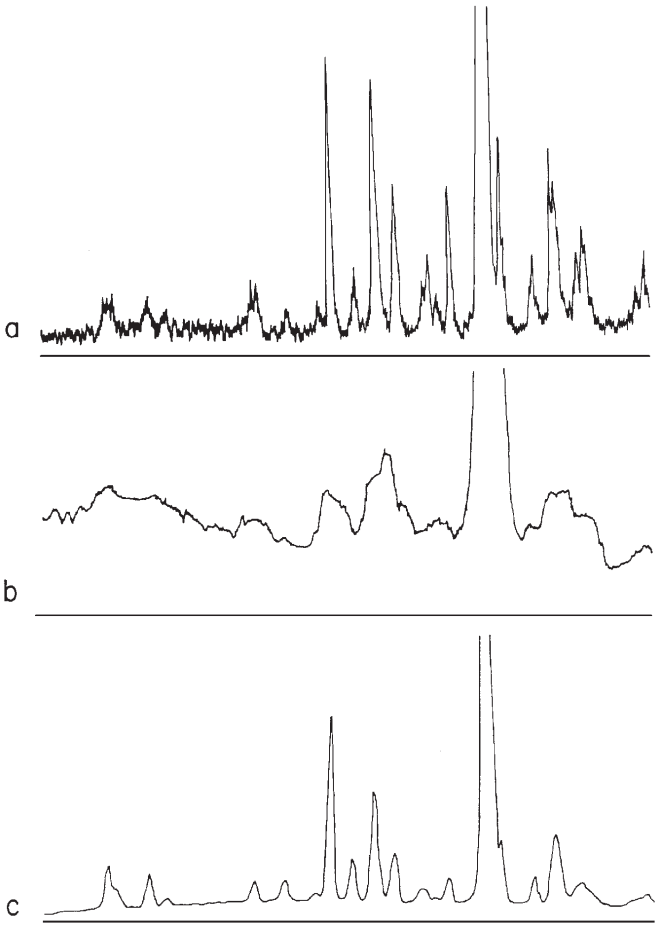

Fig. 4. X-ray diffraction pattern of a flat anorthosite specimen in two different settings (a and b) and a neutron-diffraction pattern of a cube shaped specimen (c) as sum diagram over all sample orientations; Wenk *et al.* (1986).

3. Pole figures from X-ray and neutron diffraction

Representations of experimental pole figures are generally obtained in 4 steps: (1) by measuring X-ray or neutron-diffraction patterns for a variety of different sample orientations using, conventionally, an Eulerian cradle with its (φ, χ)-sample settings (Fig. 3) or, depending on the type of diffractometer, a special sample goniometer (see chapter 4.), (2) followed by conversion of the individual sample orientations into pole-figure coordinates (α, β), (3) by points interpolation in an almost equispaced (α, β)-grid in the pole-figure projection (see Fig. 3), and (4) by graphically representing the pole figure(s) with the assigned reflection intensities.

The advantages and drawbacks of either technique, X-ray and neutron diffraction, are obvious. Texture within a polycrystalline aggregate is a statistical description of crystallite orientations and therefore requires a large number of crystallites or grains in order to get a meaningful sampling. For reproducible pole figures, numbers of 10^4 to 10^5 grains are good figures. The well-known properties of X-rays, large absorption in the sample and a small beam diameter limit their use to (1) small and thin samples, and (2) fine-grained material with grain sizes less than 10-20 μm. These limitations lead to study only the surface of a sample because X-rays penetrate the sample just from a few to several micrometres, in geological samples. X-rays measure the local texture at the sample surface. Due to the high and orientation-dependent absorption and limitations by defocusing (peak broadening by different cross-sections of the reflected beam) of Bragg reflections (compare Fig. 4 a and b) when inclining a flat sample, only incomplete pole figures can be obtained. These drawbacks, however, can be partly overcome by

clever scanning techniques, *e.g.*, combinations of measurements in transmission and reflection geometry, as well as by sophisticated data analysis. In general, X-ray diffraction is limited to monomineralic aggregates of orthorhombic or higher crystal symmetry.

Neutron beams, on the other hand, are large, up to 100 x 50 mm^2 across, and in general little absorbed in most materials. Compared to X-ray photons, neutrons are absorbed by less than three orders of magnitude (compare Table 1) and are therefore in need of large sample amounts. While this may be a drawback in many investigations, it is of great advantage in texture analysis, and especially when investigating geological materials where the global texture of the total volume has to be explored (and not only the surface texture). Due to their ability to penetrate matter and due to their large beam cross-sections, neutrons are well suited for the analysis of the bulk of a thick sample of several cm dimensions. Thus, it becomes possible to study also coarse-grained material, with grain sizes ranging up to millimetres, with reasonable grain statistics (Fig. 5). Neutron measurements can be performed in the transmission geometry on spherical, cylindrical or even irregularly shaped specimens and complete pole figures are obtained from a single scan without applying any intensity corrections (Fig. 6). The preparation of texture samples for

Table 1. Comparison of the transmission of X-rays and neutrons in minerals expressed by the penetration depths $d_{1/2}$ indicating a reduction of the transmitted intensities by a factor 2 (according to Brokmeier, 1994).

Minerals	$d_{1/2}$ [µm] X-rays, Cu$K\alpha$	$d_{1/2}$ [µm] neutrons, λ = 1.0 Å
Albite	81.0	24800
Amphibole	25.0	9690
Anhydrite	31.7	24080
Biotite	18.1	6410
Calcite	36.0	19800
Corundum	56.1	18590
Epsomite	175.1	1410
Galena	4.3	27930
Graphite	668.2	11050
Gypsum	48.5	2400
Halite	42.0	8140
Hematite	6.0	9160
Kaolinite	89.6	3040
Kieserite	79.0	3200
Magnetite	5.9	9290
Muscovite	57.9	7940
Polyhalite	38.0	6000
Pyrite	7.1	17530
Quartz	75.9	24300
Sphalerite	24.4	43600

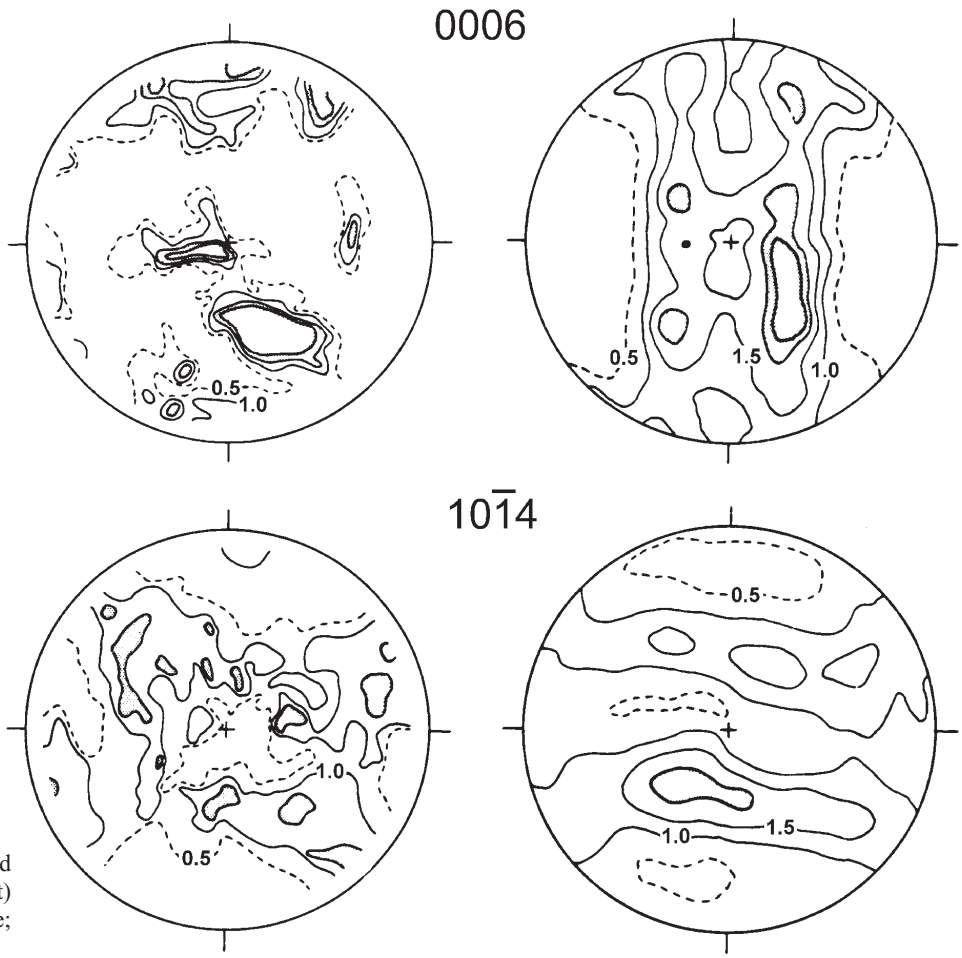

Fig. 5. Comparison of X-ray (left) and neutron-diffraction pole figures (right) for a coarse-grained deformed marble; Wenk *et al.* (1984).

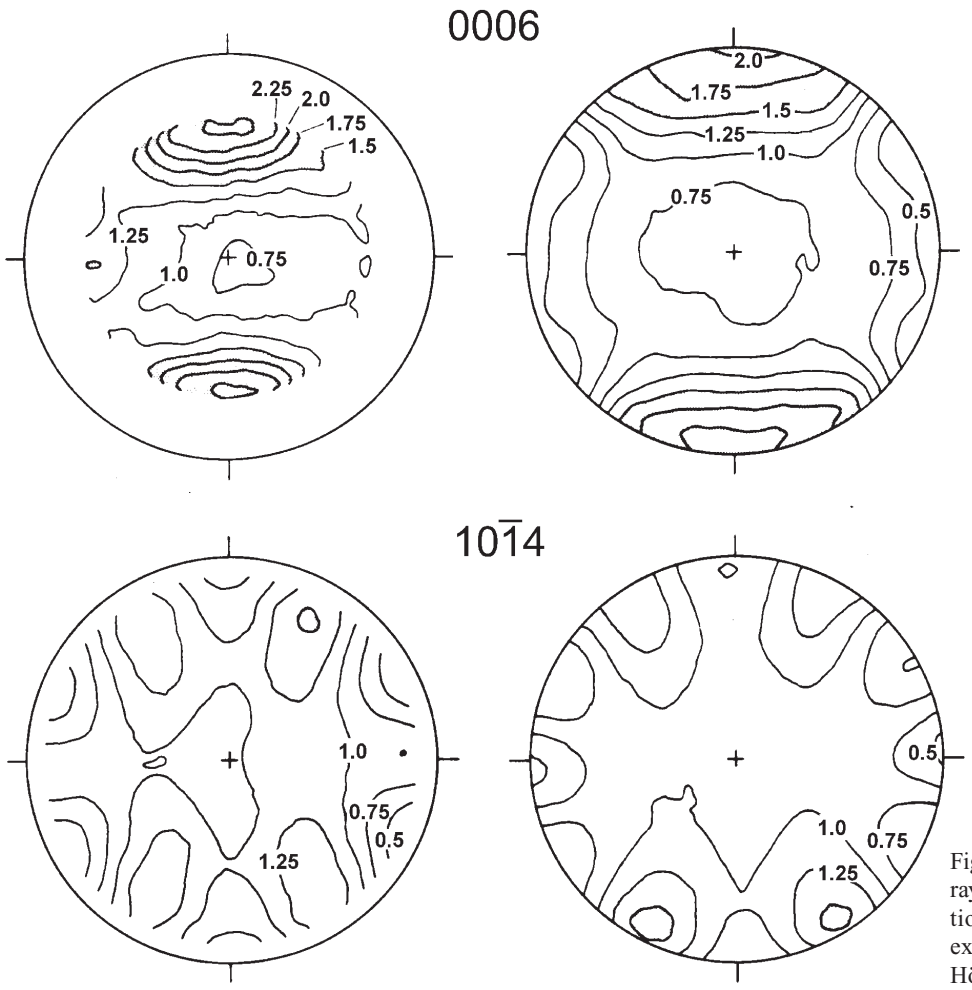

Fig. 6. Comparison of incomplete X-ray (left) and complete neutron-diffraction pole figures (right) for an experimentally deformed limestone; Höfler *et al.* (1986).

neutron diffraction is quite easy, as polishing is not necessary and surface effects (*e.g.*, roughness) can be neglected. To conclude, according to Bunge (1986), neutron-diffraction measurements with regard to texture analysis can be carried out at a much higher degree of accuracy than other techniques to calculate the orientation-distribution function.

Texture analysis of geological material is often complicated because of reflection-rich diffraction patterns of multi-phase rocks and/or mineral phases of low structural symmetry. These diffraction patterns contain a large number of reflections which are partly or strongly overlapped.

Peak overlap is more severe in neutron than in X-ray diffraction due to the disadvantage of neutrons in d-spacing resolution. Instrumental peak widths (see chapter 5.1) are intrinsically larger, *e.g.*, due to larger mosaic spreads of monochromator crystals for primary beam intensity needs considering the rather modest neutron fluxes compared to those from X-ray sources. Also for intensity reasons, neutron experiments require longer measuring times. The limited availability of neutron instruments and beam time impedes the application of neutrons in texture analysis especially when suites of different samples need to be investigated.

For a successful texture analysis of low-symmetry minerals in rocks, several requirements have to be fulfilled: (1) A large number of individual experimental pole figures is necessary to calculate the orientation-distribution functions of the different mineral constituents. Therefore, (2) extended portions of the diffraction diagrams and total peak profiles must be measured in order to record many peaks and recognize composite ones. (3) Overlapping peaks occurring in medium-resolution neutron diffraction have to be deconvoluted, *e.g.*, by mathematical procedures of peak-profile analysis (see chapter 5.). With respect to these requirements neutron diffraction offers unique advantages (a) by the use of large linear or area position-sensitive detectors and/or (b) by the application of advanced time-of-flight diffraction technologies at pulsed neutron sources.

4. Types of neutron texture diffractometers

Neutron texture diffractometers are operated in the conventional constant-wavelength mode with steady-state reactors and, using time-of-flight techniques, with pulsed neutron sources. In the following, different types of instruments will be presented. Special advantages and drawbacks are discussed.

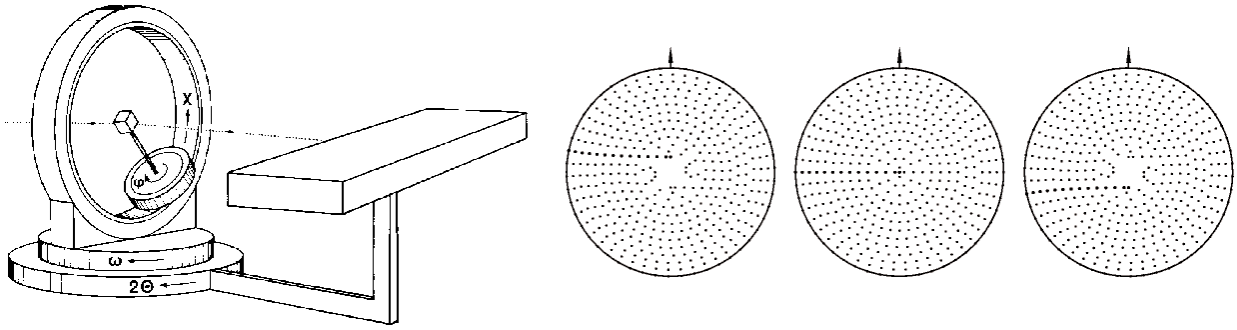

Fig. 7. Schematic view of linear detector installation at a texture diffractometer (left): Pole-figure scanning grids (right) of reflections measured in the centre (middle) and at the outer parts (left and right) of the linear detector.

4.1 Steady-state neutron sources

4.1.1 Single-counter instrument

The simplest instrumental set-up at a thermal beam tube of a steady-state reactor corresponds to that of a conventional four-circle diffractometer equipped with a Eulerian cradle as sample goniometer and a single-counting tube, *i.e.*, an instrument as it is used for single-crystal structure investigations. With the detector positioned stationary in the peak maximum of a reflection, sample-orientation-dependent intensity measurements are performed, *e.g.*, in a step-scanning mode approaching an equal-area pole-figure grid (see Fig. 3). Such an instrument is TEX-2 at the GKSS research reactor FRG-1, which has been dedicated to texture analysis (on preferentially high-symmetry materials) for many years (Brokmeier *et al.*, 1998). It has to be noted that in the case of a single-detector instrument, the different pole figures necessary for an ODF analysis have to be measured one after the other, which is a rather time-consuming procedure.

4.1.2 Position-sensitive detector instruments

More adequate to geological texture investigations, as previously discussed, are instruments equipped with position-sensitive detector systems. The first instrument to be used for a texture investigation on a triclinic plagioclase was D1B at the high-flux reactor of the ILL in Grenoble (Wenk *et al.*, 1986). Many pole figures have been obtained simultaneously with the 80°-wide "banana-type" detector. Collection and processing of pole-figure data by means of a linear detector, however, have to take into account the so-called "blind area" effect (Bunge *et al.*, 1982). In normal diffraction geometry the Eulerian cradle is set up in such a way that the χ-circle coincides with the bisectrix of incident and diffracted beam. Any direction on the pole figure can be brought parallel to the bisectrix by two rotations χ and φ, which correspond to spherical coordinates α and β of the diffracting lattice plane (see Fig. 3). With a continuous detector this is true only for one 2Θ-angle ($\omega = 2\Theta/2$ in the centre of the detector). For all others, the χ circle is inclined by ω to the bisectrix. In this case, χ no longer coincides with α, nor φ with β with the consequence that there remains a blind area in the centre of the pole figure. The blind area, which is larger for reflections measured in the outer parts of the linear detector, can be experimentally overcome by collecting some additional data in different ω-settings of the Eulerian cradle.

Corresponding pole-figure scanning (Fig. 7) has been the routine operation at the dedicated texture diffractometer SV7b of the research reactor FRJ-2 in the Forschungszentrum Jülich for more than ten years (Will *et al.*, 1989; Jansen *et al.*, 2000a). SV7b (Fig. 8) is equipped with (a) a linear scintillation detector of the JULIOS-type 940 mm in length covering a stationary $\Delta 2\Theta$-range of about 50° (Schäfer

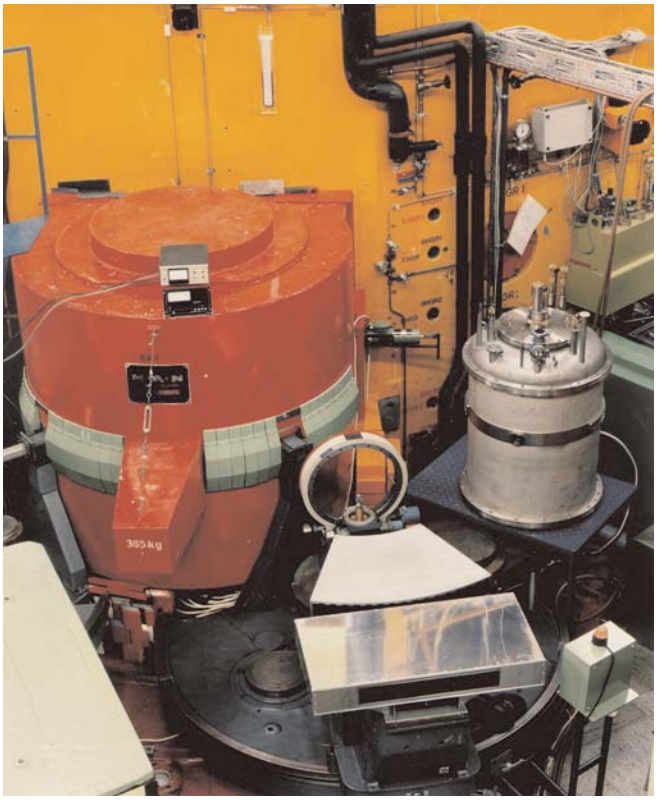

Fig. 8. Photograph of the texture diffractometer SV7b in Jülich equipped with full-circle Eulerian cradle, radial collimator and linear JULIOS detector. Alternative low-temperature Eulerian cradle with He cryostat (at the right).

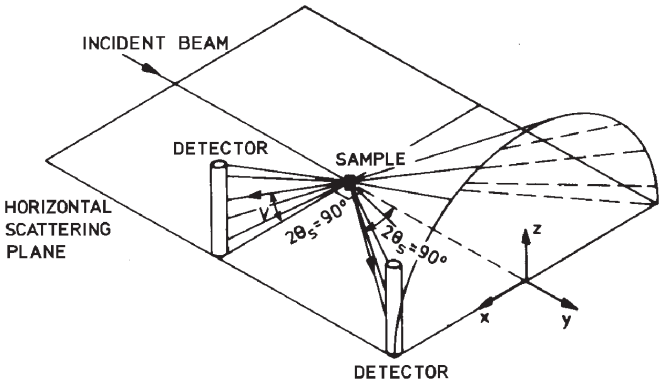

Fig. 9. Illustration of 90°-scattering geometry (detector at $2\Theta_s$ = 90°). The Debye-Scherrer cone degenerates to a plane and the detector axis lies completely in this plane (perpendicular to the horizontal scattering plane); Jensen (1986).

et al., 1995b) and (b) an alternative set-up of Eulerian cradles, a conventional one for room temperature measurements and a special one mounted inside a He cryostat for low-temperature studies (Elf *et al.*, 1990). Due to its position-sensitive detector this instrument has been and is operated as a service instrument mainly for geological texture investigations (*e.g.*, Ghildiyal *et al.*, 1999; Will *et al.*, 1990; Jansen *et al.*, 1992; Schäfer *et al.*, 1992; Siemes *et al.*, 1993; Jansen *et al.*, 1993, 1999, 2000b; Gastreich *et al.*, 2000).

4.1.3 Vertical detector set-up

An alternative position-sensitive detector set-up was used at the TAS3/TAS6 instrument at the DR3 reactor in Risø (Jensen & Kjems, 1983). The linear detector is mounted with its axis vertical in order to record part of the χ range of a single reflection at once. In a fixed $2\Theta = 90°$ position the Debye-Scherrer cone degenerates to a plane perpendicular to the incident beam, and the detector axis lies completely in this plane and the neutron path to the detector has the angular range for equal length. (Fig. 9). For each reflection, however, the appropriate wavelength has to be chosen, thus limiting this set-up at a stationary neutron source to reflection-poor patterns of high-symmetry materials. The potential of this equipment lies in the fast measurement of a pole figure thus allowing the study of texture kinetics, *e.g.*, during *in situ* recrystallization, even at a medium-flux continuous reactor source (Jensen, 1992).

4.2 Pulsed neutron sources

4.2.1 Time-of-flight technique

Time-of-flight (TOF) diffraction with a pulsed source is an alternative technology to construct and operate diffractometers. According to Bragg's law

$$d = \frac{\lambda}{2\sin\Theta} \tag{4}$$

d-spacing patterns, which with a continuous source are collected by applying the conventional angle-dispersive method (variation of the instrumental parameter Θ) at a constant wavelength λ, are here recorded by using the wavelength- (or energy-) dispersive method (variation of the instrumental parameter λ) at fixed scattering angle(s). Different wavelengths of a white neutron beam relate to neutron velocities *v* by the de Broglie relation

$$\lambda = \frac{h}{m \cdot v} \tag{5}$$

where *h* denotes Planck's constant and *m* the neutron mass. For a given total flight path *L* from source to detector, the neutron velocity and thus its kinetic energy is obtained by the measurement of the flight time *t* assuming that the neutron was elastically scattered by the sample:

$$v = \frac{L}{t} \tag{6}.$$

Combining (5) and (6) with Bragg's equation (4) yields a direct relation between time-of-flight and crystallographic d-spacing

$$d = \frac{h}{2m} \cdot \frac{t}{L \cdot \sin\Theta} = \frac{t}{505.56 \cdot L \cdot \sin\Theta} \tag{7}$$

in which *t* is measured in microseconds, *L* in meters and d in Å. Thus, for a given flight path *L* and any single detector tube (or detector channel) at a scattering angle 2Θ the TOF measurements yield a diffraction pattern in the form of intensities versus d-spacing.

4.2.2 Multi detector set-up

The adaptation and suitability of the TOF measuring technique to quantitative texture analysis was firstly proven with the high-flux pulsed reactor IBR-2 at Dubna, Russia (Feldmann *et al.*, 1980). The dedicated TOF texture diffractometer NSHR has been built up by using a flexible horizontal multi detector arrangement allowing the simultaneous recording of different pole figures in a reasonable time, especially in the field of low-symmetry and multi-phase geological material (Feldmann *et al.*, 1991). Recently, the new SKAT texture diffractometer with a flight path of about 103 m has been installed (Ullemeyer *et al.*, 1998). This instrument is characterized by an axial-symmetrical arrangement of detector-collimator modules at the unique scattering angle $2\Theta = 90°$, thus avoiding all Θ-dependent geometrical intensity corrections, although limiting the accessible d-spacing range to 5.4 Å due to pulse overlap. The detector installation on a 2π-ring allows the collection of complete pole-figure data by a single sample revolution on a one-axis goniometer in the centre of the ring.

4.2.3 Linear position-sensitive detector set-up

As of several years, the ROTAX instrument at the pulsed spallation source ISIS, Rutherford-Appleton Laboratory, U.K., has been operated as a multipurpose powder and texture diffractometer (Schäfer *et al.*, 1995a) equipped with continuous position-sensitive JULIOS-detectors (Schäfer *et al.*, 1995b). The operation mode as an angle-dispersive TOF diffractometer with a neutron flight path of about 15 m

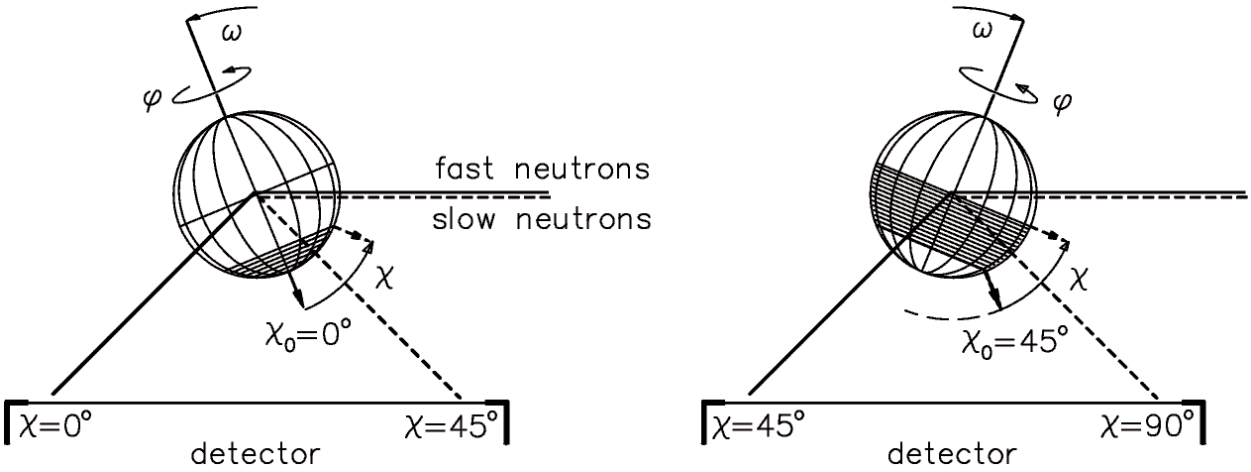

Fig. 10. The pole-projection sphere in two different χ_0-settings corresponding to an extension of $2\Theta = 90°$ of a linear detector. Left: Fast neutrons reflected by Bragg-planes perpendicular to $\chi = 0°$ reach the left part of the detector, slow ones reflected from Bragg planes of the same d-spacing but perpendicular to $\chi = 45°$ arrive on the right side. Right: A different χ_0-setting results in the reflection of differently oriented planes; Jansen *et al.* (1996a).

allows an efficient exploitation of the polychromatic neutron spectrum (Schäfer *et al.*, 1993). Using a polychromatic beam and a linear detector, Bragg reflection conditions are fulfilled for different wavelengths at different positions of the detector. Thus, the reflection of a given {hkl} can appear along the total length of the detector due to the wavelength-dependent scattering angle, and different orientations of one Bragg plane can be seen simultaneously at different positions of the linear detector. Because of this, it is possible to replace a scan, necessary at a constant-wavelength diffractometer, by the angular extension of the detector (Fig. 10). A linear dimension of the detector covering 90° in 2Θ corresponds to a $\Delta\chi$ coverage of 45° of the sample. Then two different turn-table settings $\omega = \chi_0$ are necessary to cover all pole distances χ of one hemisphere (Fig. 11). It should be noted that the combination of white-beam TOF technique and the use of a linear detector meets two objectives simultaneously: (1) the reduction of sample orientations in the course of pole-figure scanning and (2) the simultaneous measurement of a multitude of different (hkl) pole figures. This gain in pole-figure data-collection times up to a factor of 50, as compared with conventional constant-wavelength diffraction (Jansen *et al.*, 1996b; Schäfer *et al.*, 1997), has a trade-off in a more complex way of extracting pole figures from the measured data. A rather sophisticated procedure in data processing and analysis has been developed for this purpose (Jansen *et al.*, 1996a).

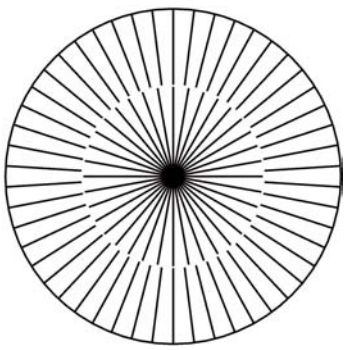

Fig. 11. Traces of the detector on the pole projection sphere during a χ_0/φ-scan with two χ_0 settings (equal area projection).

4.2.4 Area detectors and three-dimensional set-ups of detector banks

Texture analysis using TOF diffraction and two-dimensional detector arrays have been developed at the pulsed

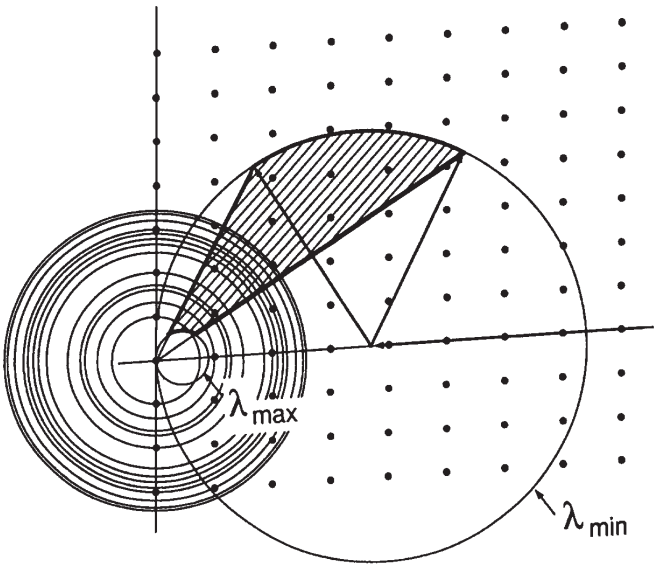

Fig. 12. Section of reciprocal space of single crystal (dots) and powder diffraction (circles). The range between minimum and maximum wavelength can be covered within the range of the detector (shaded region); Wenk *et al.* (1991).

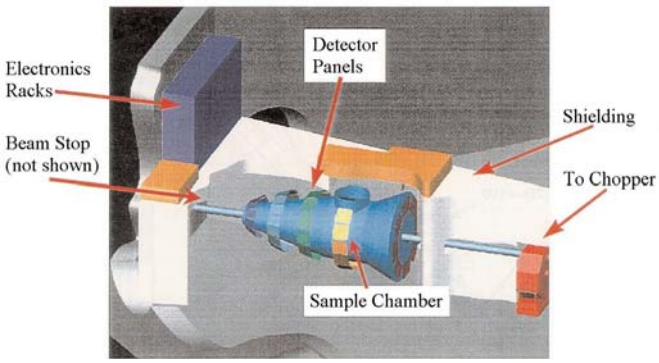

Fig. 13. Beam layout for HIPPO with sample chamber and detector panels in forward, 90° and backscattering geometry; Bennett *et al.* (1999).

spallation sources of LANSCE at Los Alamos National Laboratory, USA, and IPNS at Argonne National Laboratory, USA. Different pole-figure scannings have been performed by various sample settings on diffractometers originally designed for single-crystal diffraction (Fig. 12) differing in sample-goniometer set-up and type of area detector. Pole-figure results are given in comparison to those obtained at conventional reactor instruments (Wenk *et al.*, 1991). Actually, a state-of-the-art high-pressure preferred-orientation diffractometer HIPPO is under construction at Los Alamos (Bennett *et al.*, 1999). The high-intensity TOF diffractometer features a short initial flight path of 9 m and will be used primarily for high-pressure and texture studies. It is characterized by a novel three-dimensional arrangement of detector banks with 1400 He tubes, on five conical rings at 2Θ-positions of 10°, 20°, 40°, 90°, and 150° respectively (Fig. 13). The d-range is from 0.5 to 9.0 Å. A conventional 3-axis goniometer using Kappa geometry will be used for standard texture measurements. A single sample setting will give considerable coverage of the orientation space (Fig. 14). A 32-sample changer will allow quick texture analysis of multiple samples which is important for systematic investigations of larger series of geological specimens. Operation at a wide range of pressure and temperature conditions will make it possible to conduct *in situ* dynamic measurements of reactions, deformations and recrystallization.

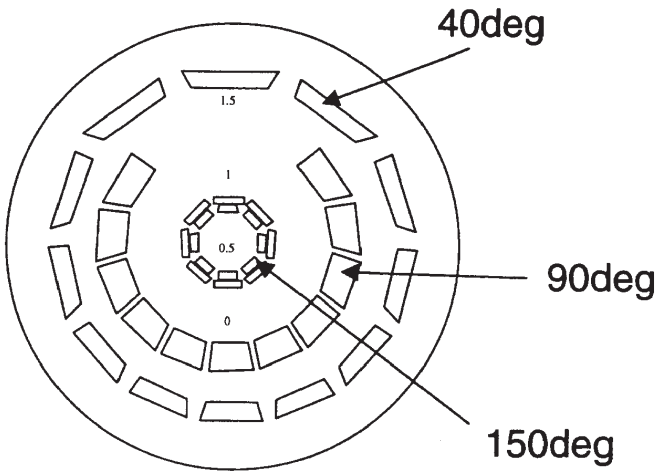

Fig. 14. Stereographic projection of the 150°, 90° and 40° sets of detector panels on a pole figure for a single sample orientation. Incident beam direction is along the projection axis. The gap in the 90° detector panel image arises from the sample chamber access port in the 90° detector bank. The detector panel images for the 150° and 40° have no gaps; Bennett *et al.* (1999).

5. Individual pole figures by pattern decomposition

The crucial point in the diffraction-data analysis of geological material is the peak overlap in diffraction patterns of low-symmetry and multiphase materials hindering or even making it impossible (in case of single-counter instruments) to obtain individual pole figures. To overcome these difficulties, total peak profiles must be recorded by using position-sensitive detectors in order to have a chance to recognize superimposed peaks and to deconvolute them by mathematical procedures of peak-profile analysis. The analysis of a diffraction pattern can be pursued by two different approaches: the "Rietveld method" (Rietveld, 1969), *i.e.*, a full-pattern profile-fitting procedure starting with random texture and structure models of all phases of the material (see chapter 11 for different approaches), or by a flexible decomposition of selected peak clusters or parts of the diffraction pattern for the determination of integrated intensities (Jansen *et al.*, 1988). This approach is performed by profile fitting on a two-step basis (Schäfer *et al.*, 1991) with the determination of (1) global structural parameters and, subsequently, of (2) texture specific parameters in the form of orientation dependent integrated intensities to be used for pole-figure representation.

5.1 Neutron-diffraction peak profiles

The observed diffraction pattern originates from the true diffraction effect of the specimen modified by geometrical and instrumental aberrations and the intensity distribution of the neutron source. The profile analysis of a diffraction pattern must take into account the convolution of instrumental and sample parameters. The peak shape depends primarily on the radiation source and the wavelength distribution of the primary beam and is further influenced by instrumental components like monochromator crystals, slits, collimator arrangements and the detector system. Due to the statistics and the velocity distribution of reactor neutrons and due to the mosaic distribution of the monochromator crystals, the profile of a diffraction peak at a reactor is well described by a pure Gaussian function

$$G(2\Theta) = H \exp\left\{-4 \ln 2 \left(\frac{2\Theta - 2\Theta_p}{FWHM}\right)^2\right\} \qquad (8)$$

defined by the three parameters peak position $2\Theta_p$, peak height H and full width at half maximum FWHM (Fig. 15). G describes the neutron intensity at an arbitrary scattering angle 2Θ of a Bragg reflection centred at $2\Theta_p$. The corresponding peak profile at a spallation source, however, is

asymmetric (Fig. 15) and can be modelled by three different sections: a fast Gaussian-type increase, a slower Gaussian-type decrease, and a very slowly decreasing exponential-type tail. In the following, considerations will be restricted to reactor conditions. The variable FWHM is strongly 2Θ dependent and its functional dependence can be described by the analytical expression (Caglioti *et al.*, 1958)

$$\mathrm{FWHM} = \sqrt{U\tan^2\Theta + V\tan\Theta + W} \qquad (9)$$

with the instrumental parameters U, V and W. These parameters define the so-called instrumental function which can be derived experimentally, together with other instrumental parameters like wavelength and zero-shift of the detector, by collecting diffraction patterns of standard sample material, *e.g.*, silicon, corundum, and mica (Jansen *et al.*, 1988, 1986). Instrumental peak broadening can be superimposed by sample broadening due to microstructural imperfections resulting from macro- and microstrains (compare chapter 8) and particle-size effects. A rough criterion is that strain and size broadening can be described by Gaussian and Lorentzian profile shapes, respectively. Resultant profile functions are discussed *e.g.*, by de Keijser *et al.* (1983).

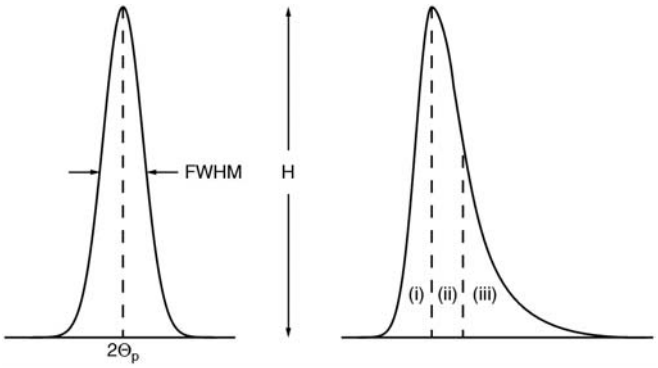

Fig. 15. Symmetric Gaussian profile of a Bragg peak from reactor neutrons (left) and asymmetric peak profile of spallation source neutrons (right). The Gaussian peak is defined by position $2\Theta_p$, full width at half maximum FWHM and peak height H. The asymmetric peak profile can be divided in three regions (i), (ii), (iii) (see text).

5.2 Two-step procedure in profile fitting

The first step in data analysis of pole-figure scans is concerned with the evolution of global parameters which are valid for all sample orientations, *i.e.*, independent of the texture. Global parameters are in the first place positions $2\Theta_p$ of the Bragg reflections which are directly correlated to the d-spacings of the structure. The determination of the global parameters is performed on a sum-data set which is generated by adding up the individual diffraction patterns of all sample orientations. One should keep in mind, however, that this summation averages out peak shifts due to residual stresses or positioning errors. This sum-data set is characterized by very good statistics as it represents the scattered intensity from the sample during the total data-collection time.

The profile fit of the sum diagram is performed by using an interactive program, *e.g.*, PROFAN for on-line operation on a graphic display (Merz *et al.*, 1990). The program contains routines for the background determination of the diffraction pattern. For this, three different methods are provided: a polygon or a spline fit through footing marks to be selected manually with the cursor, or a determination based on a polynomial calculation in an iterative procedure. Next, PROFAN fits pre-selectable profile functions (*e.g.*, Gaussian or Pseudo-Voigt) into measured peaks or peak clusters after having segmented the diffraction pattern into suitable 2Θ sections. The profile fitting is based on a non-linear weighted least-squares routine by minimizing the sum of the weighted squared differences between observed and calculated counting rates. Profile parameters to be refined are peak positions $2\Theta_p$, half widths FWHM and heights H. The profile fitting ends with a list of refined parameter values with appropriately estimated standard deviations.

The individual, orientation-dependent diffraction patterns which may have rather poor counting statistics, depending on the measuring time used for each sample orientation during pole-figure scanning, are now used to fit the peak heights H of all reflections of interest. Again using PROFAN, this intensity analysis is based on the results obtained from the fit of the sum diagram in the first step. The data processing starts with an adjustment of the sum-data-set background function to the individual data sets by linear scaling, followed by the subtraction of the actual background. The ensuing real profile fit is reduced to least-squares intensity adjustments by variation of the peak heights H for all possible reflections, based on the known $2\Theta_p$ positions and FWHM values of the sum diagram.

The integrated intensity I_{hkl} of a reflection is equivalent to the area below the profile function. In case of a Gaussian function it is expressed by the finite integral

$$I_{hkl} = H\,\frac{FWHM}{2}\sqrt{\frac{\pi}{\ln 2}} \qquad (10).$$

Individual pole figures are then constructed by assigning the individual, orientation-dependent intensities to the pole figure coordinates (α, β) as described in chapter 3.

6. Examples of mineral and rock textures analysed by neutrons

Most texture research in mineralogy and geology, so far, were done on monomineralic, naturally and/or experimentally deformed ores minerals, such as hematite, magnetite, pyrite, chalcopyrite or pyrrhotite and rocks such as quartzite and calcite as well as plagioclase (compare Wenk, 1998). In the future, however, the special potential of neutrons to isolate individual peaks in reflection-rich diffraction patterns will be used more extensively for texture investigations on polymineralic, deformed materials being by far the most naturally occurring rocks. One

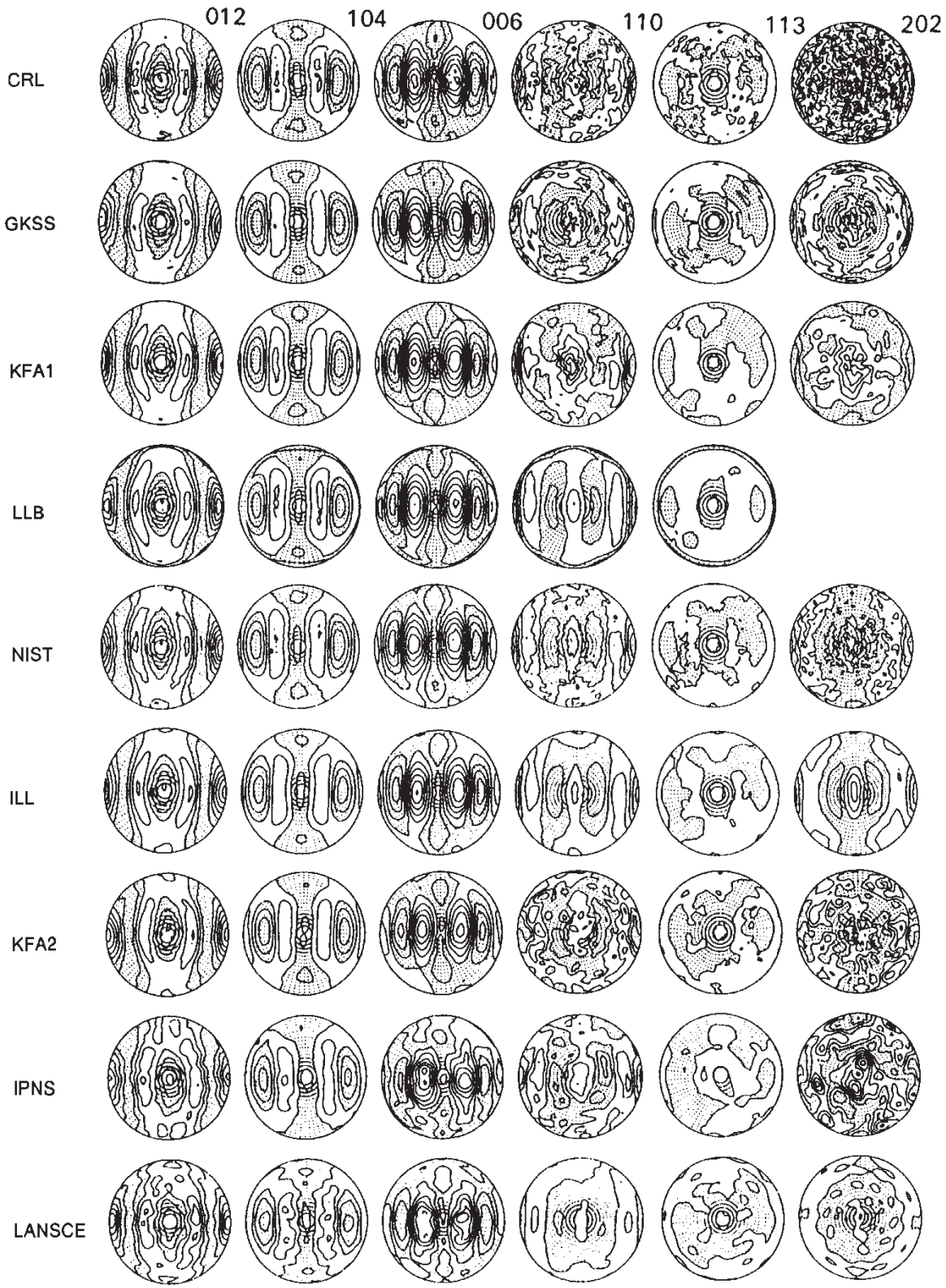

Fig. 16. (a): Experimental pole figures of the limestone standard sample measured at nine facilities, contour interval is 0.2 m.r.d..

example is granite, consisting of feldspar, quartz and mica. Very recently, investigations on an orthopyroxene-sillimanite-granulite were reported (Gastreich *et al.*, 2000). Neutron-diffraction pole-figure data can be collected in variable sample environments, *e.g.*, at 77 K on deformed ice polycrystals thus providing detailed views of icy bodies

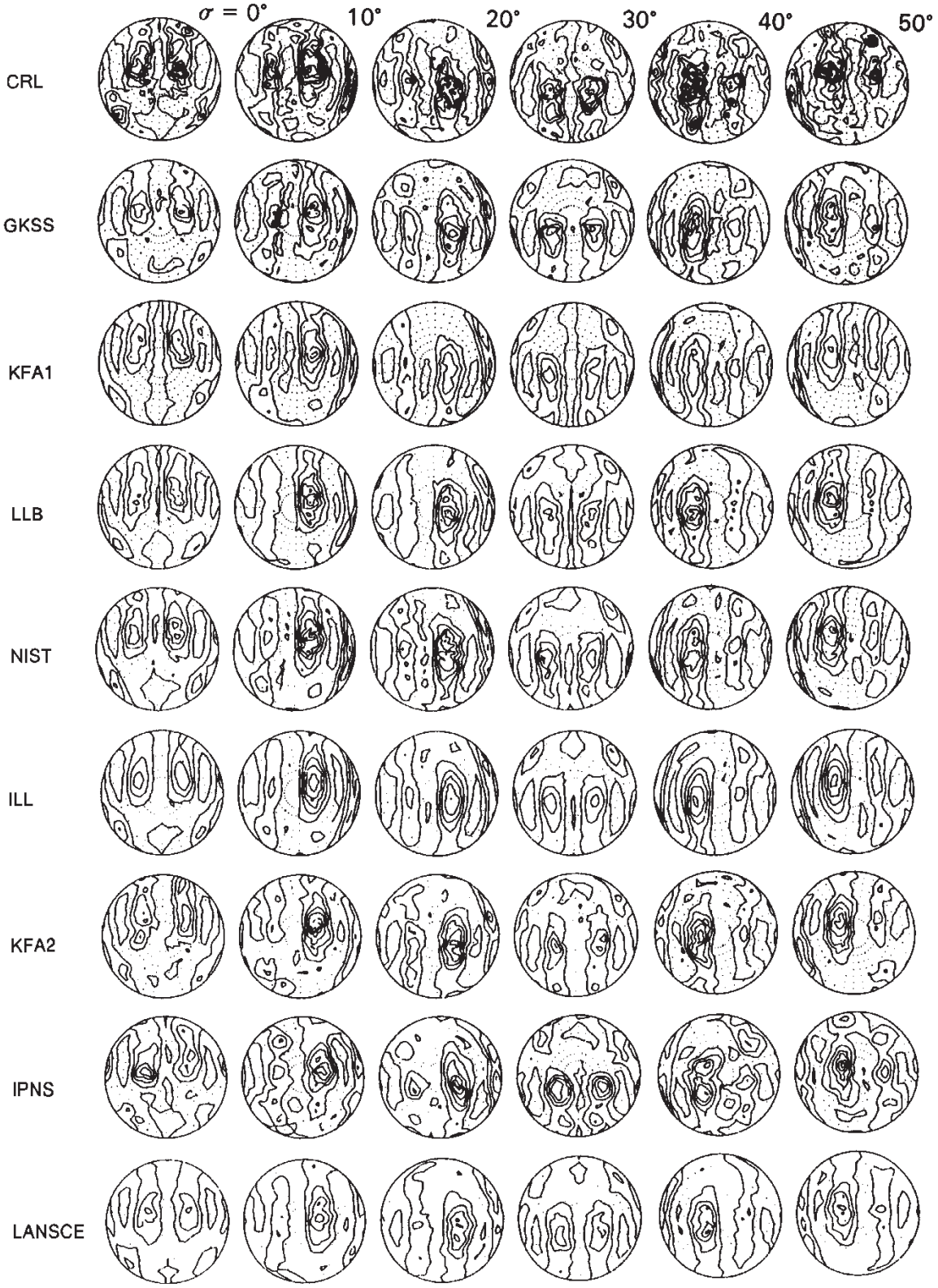

Fig. 16. (b): Orientation distribution calculated with the WIMV algorithm (Matthies *et al.*, 1988) from six experimental pole figures represented as $\sigma = (\alpha+\beta)/2$ sections; contour interval is 0.5 m.r.d.; Helming *et al.* (1988).

of outer solar systems. The application of neutron diffraction is non-destructive and does not require cutting of rare or unique pieces such as meteorites.

In the following, some results of neutron-diffraction texture investigations on above-mentioned geological materials are presented. The examples selected are by no

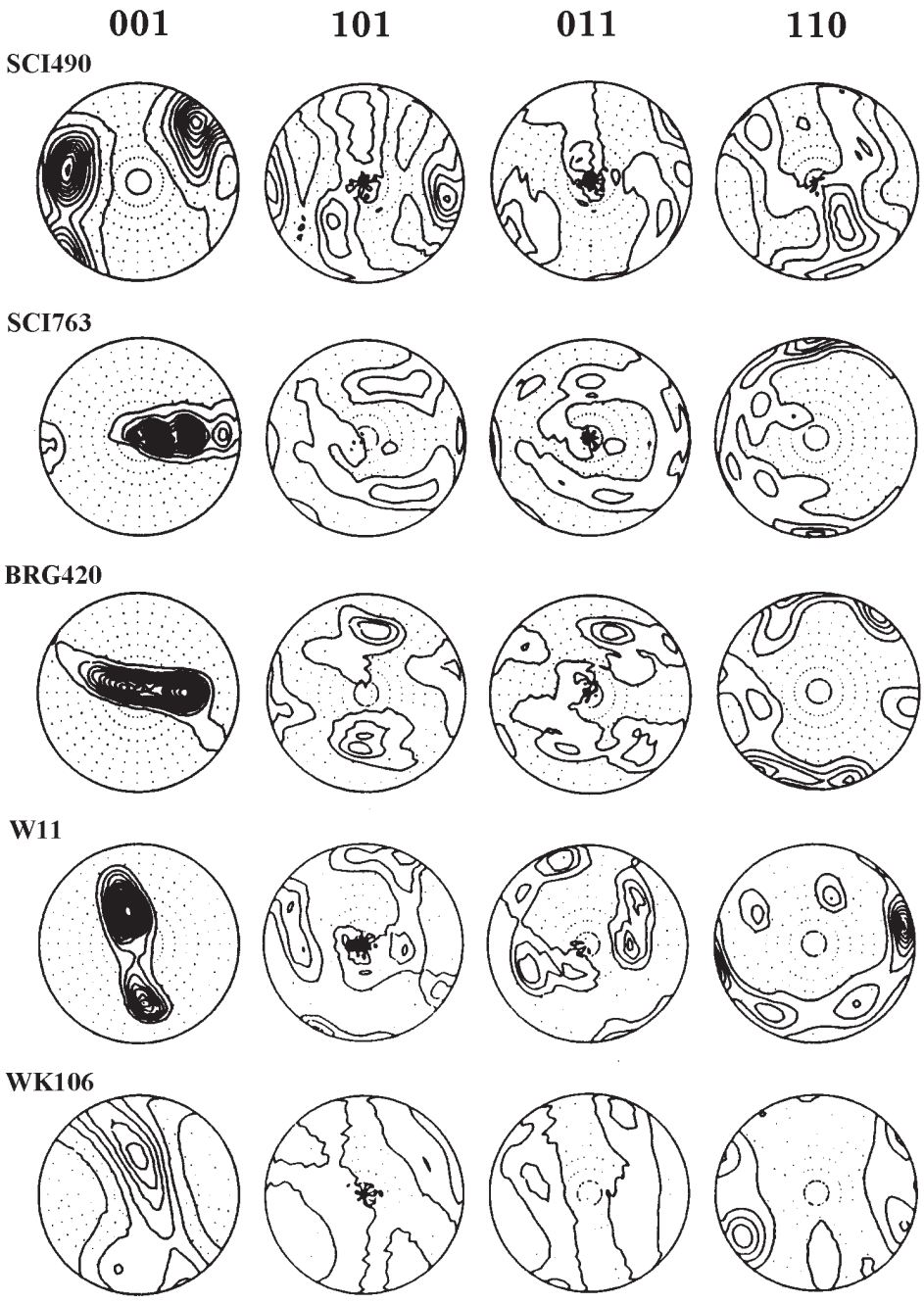

Fig. 17. Calculated pole figures obtained from an ODF analysis of experimental pole figures of naturally deformed quartzites SCI490, SCI763 and BRG420 from the Bergell Alps and W11 and WK106 from South-East California. Contour intervals 1.0 m.r.d.

means intended to be exhaustive but they are representative for a variety of applications.

6.1 Calcite

About ten years ago, a basis for quantitative texture analysis has been provided by a round robin standard project for the determination of pole figures by neutron diffraction (Wenk, 1991). In an effort to evaluate the reliability of experimental pole figures, a mineral sample of polycrystalline calcite was circulated among nine neutron-diffraction facilities, with reactor and spallation source instruments, single-tube and position-sensitive detector installations, therefore involving constant wavelength and time-of-flight techniques. The study was extended with additional data from Dubna, Russia (Walther *et al.*, 1995). The sample was a fine-grained natural limestone with a random orientation distribution, almost pure calcite $CaCO_3$, which had been artificially deformed in pure shear to a strain $E_1 = 35$ %, $E_2 = -3$ % and $E_3 = -36$ %. The D20 beam line at ILL has also provided results on the limestone standard, though not published in an international review, but accessible in the ILL reports.

The experimental pole figures were normalized to express densities in multiples of a random distribution

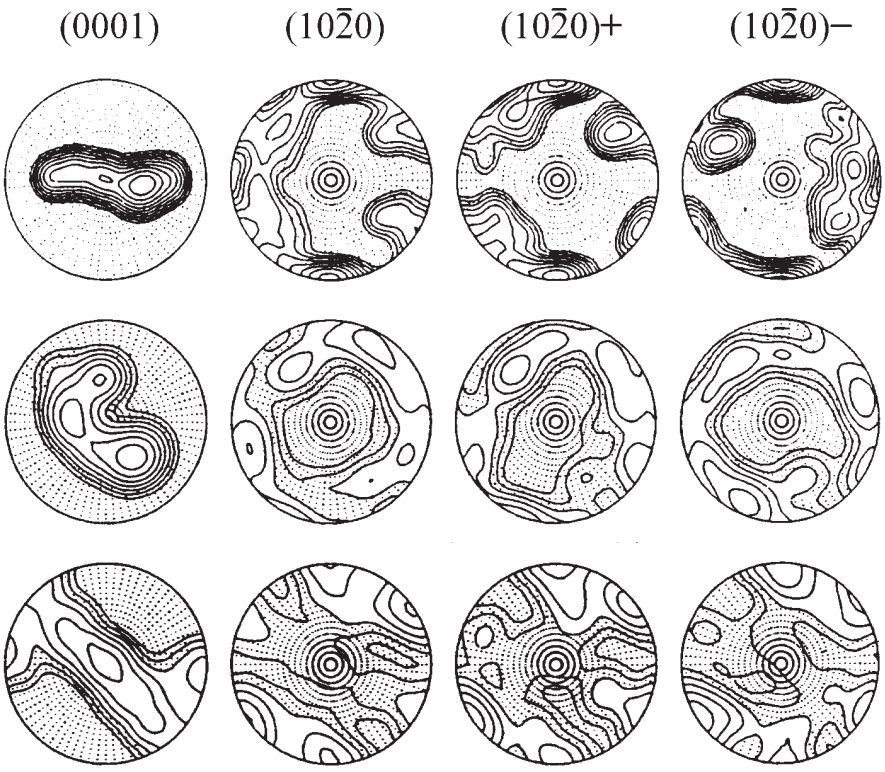

Fig. 18. Reduced pole figures of three types of quartz textures as summation over the pole figures of several samples after visual rotation into a similar orientation: type 1 (top) summation over 5 individuals, type 2 (centre) summation over 2 individuals, and type 3 underrepresented by only one individual; Helming *et al.* (1994).

(m.r.d.). These pole figures as well as the three-dimensional orientation distribution represented as a density distribution of Euler angles are shown in Fig. 16. In general, textures agree very closely. For pole figures with strong diffraction intensities, mean standard deviations are 0.04-0.06 m.r.d. with a spread of maxima values of 0.18 m.r.d. The spread is considerably larger for pole figures with weak diffraction intensities, *e.g.* (110), and so are standard deviations (0.20 m.r.d.). For weak diffraction peaks, position-sensitive detectors have an advantage over single-tube detectors due to the collection of integrated intensities beyond the total peak profiles.

Calcite rocks (limestone and marble) are a good model system for experimental rock deformation. Since calcite rocks are mechanically relatively ductile compared to other minerals, high confining pressure is not necessary and therefore deformation experiments other than uniaxial compression can be performed more easily. In a recent study with the SKAT time-of-flight texture diffractometer at Dubna, equipped with a chamber for uniaxial compression and high temperatures, an attempt was made to determine textural and structural changes of calcite marble depending upon the temperature and mechanical stresses, as well as depending upon the time of load (Ivankina *et al.*, 1999). Distinct texture changes were only observed after long-time exposure under load for 20 weeks. The observed smoothing of the contour lines in the pole figures is attributed to grain-size reduction. The pole-figure results indicate dynamic recrystallization in response to long-acting stress at low temperatures.

6.2 Quartz

Natural quartz textures, in contrast to calcite textures, display a wide variation and low symmetry. This may be due to changes in mechanisms such as dislocation glide, climb and recrystallization, but also due to differences in the deformation history. Fig. 17 illustrates pole figures of some typical quartz textures obtained by measurements on the neutron texture diffractometer in Jülich on ten naturally deformed metamorphic quartzites from various locations and different geological settings (Schäfer *et al.*, 1992). The experimental pole figures were decomposed into components (Helming, 1996) for a compact description of the texture.

One recognizes basically three types of textures (Helming *et al.*, 1994) from which two types are well represented (Fig. 18). The first type is characterized by a more or less asymmetric (triclinic) double maximum of c axes in the foliation plane and at high angles to the lineation. The a axes usually concentrate in a maximum near the lineation but this is much less defined. The second texture type is represented by an incomplete small-circle girdle of c axes about the pole of schistosity. This texture is similar to one described from regionally metamorphosed gneisses. The third type shows an oblique great circle of c axes, also with a maximum normal to the lineation.

From the component analysis of the different textures, Dauphiné-twin-related orientations are recognized in the fabrics with a c axis maximum. It should be emphasized, however, that the component method has been used in a

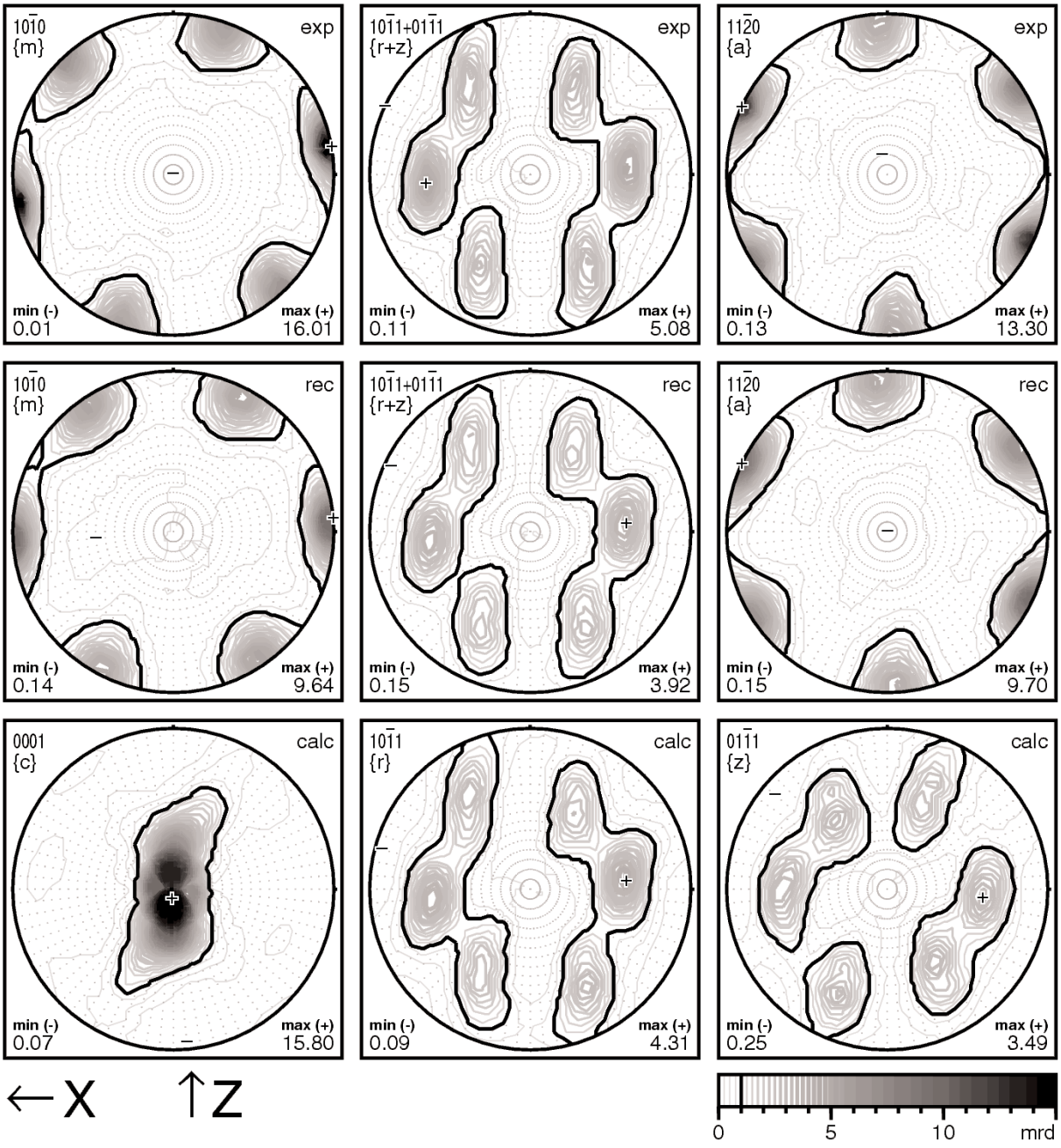

Fig. 19. Observed and calculated neutron pole figures of a quartzite. *Top row:* experimental pole figures {m}, {r+z}, and {a.}. *Second row:* corresponding model pole figures recalculated from the ODF. *Bottom row:* calculations of the "unobserved" pole figures {c}, {r}, and {z}; Ghildiyal *et al.* (1999).

purely descriptive way without correlating components to deformation mechanisms, except to infer twinning. At present, there is no interpretation for the texture types and particularly for the triclinic symmetry of most pole figures. Simple shear, which is clearly involved, should produce monoclinic pole figures as they are observed in carbonates and phyllosilicates.

Recently (Ghildiyal *et al.*, 1999), the deformation mechanisms of a deformed quartzite from the Kakao belt, North-West Namibia, have been described from neutron-diffraction volume-texture measurements and ODF calculations using the program MENTEX allowing the calculation of the "unobserved" pole figure of the base pinacoid {c}, and the separation of the intrinsically overlapped pole figures of the positive and negative rhombs {r} and {z} (Fig. 19). The distribution of the c axes along the girdle suggests that the rock deformation was predominantly by prism slip under the influence of simple shear component, *i.e.*, with a contribution of the slip along the rhomb and basal planes. Poles of the positive and negative rhombs

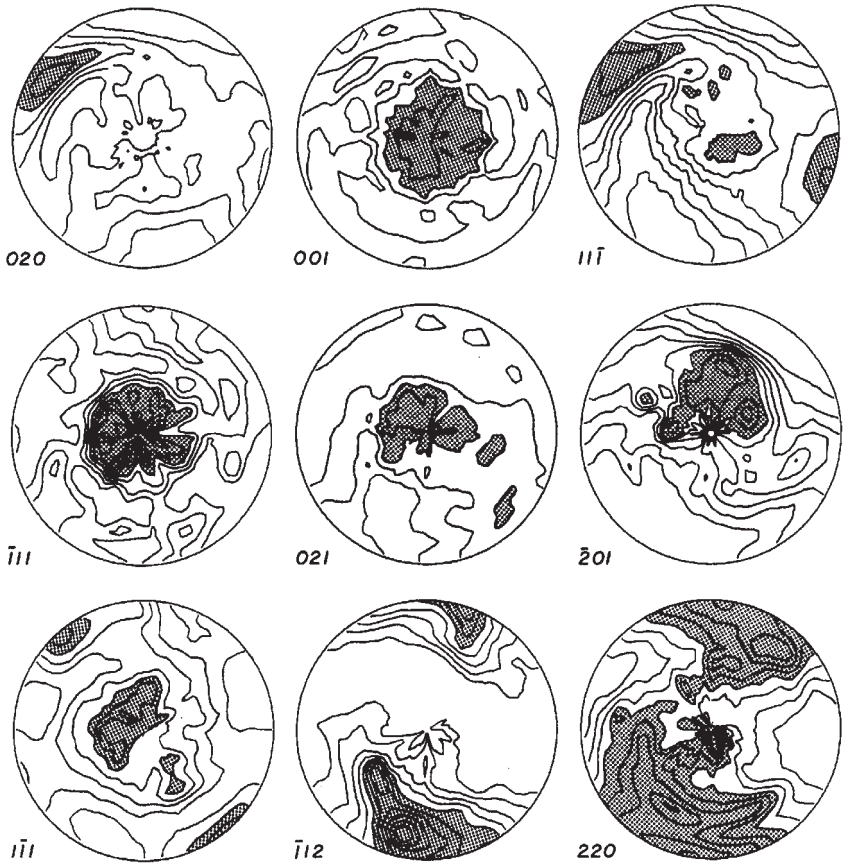

Fig. 20. Selection of separated pole figures of San Juan anorthosite. Projection is on the schistosity plane. Contour intervals 0.1 m.r.d., shaded above 1.2 m.r.d.; Wenk *et al.* (1986).

show a tendency of symmetry in their alignment with respect to the shear plane.

6.3 Plagioclase

Plagioclase together with K feldspar is a dominant phase in the earth's crust, but deformation mechanisms of plagioclase are hardly known. Conventional X-ray diffraction techniques have failed due to the complex diffraction pattern of the triclinic mineral. Neutron diffraction, however, succeeded already in the early days of neutron-diffraction texture analysis to measure the preferred orientation of triclinic feldspar in deformed rocks by using the linear "banana-type" detector at D1B in Grenoble (Wenk *et al.*, 1986). A total of 15 pole figures of an anorthosite mylonite from San Juan Bautista, California, was separated by peak deconvolution using profile-fitting methods (Fig. 20). All pole figures display strong preferred orientation with complicated triclinic distributions. It appears that (001) poles are concentrated normal to the schistosity plane of the specimen and that (020) poles have a maximum nearly perpendicular to the poorly developed lineation in the schistosity plane. This is consistent with x = [100] directions oriented parallel to the lineation as has been reported previously (Sander, 1950). A full description of the texture, however, failed because it was not possible to calculate a full ODF from a triclinic material, at the time of the investigation.

Several years later, two examples of quantitative neutron-diffraction texture analysis of plagioclase samples with quite different microfabrics, originating from a Precambrian high-temperature shear zone of the Jutan Nappe Complex in Norway, were reported (Ullemeyer *et al.*, 1994). The textures are described by means of components (Helming & Eschner, 1990; Helming, 1996). In both cases the results confirm the rather good compatibility of the experimental pole figures, although the degree of preferred orientation is weak. Despite large statistical errors good conformity was observed between experimental and recalculated pole figures. It is shown that the main features of the geological textures are described by a rather small number of components giving all information necessary for the geological interpretation of preferred orientations.

6.4 Pyrrhotite

Neutron diffraction is especially suited to accompany deformation experiments on natural materials with an initial preferred orientation or on ores, in which the minerals develop only very weak preferred orientation, because the bulk texture can be measured before and after the artificial deformation on one and the same specimen. Neutron diffraction has been used to investigate the development of deformation textures of polycrystalline pyrrhotite ores $Fe_{1-x}S$ (Niederschlag & Siemes,

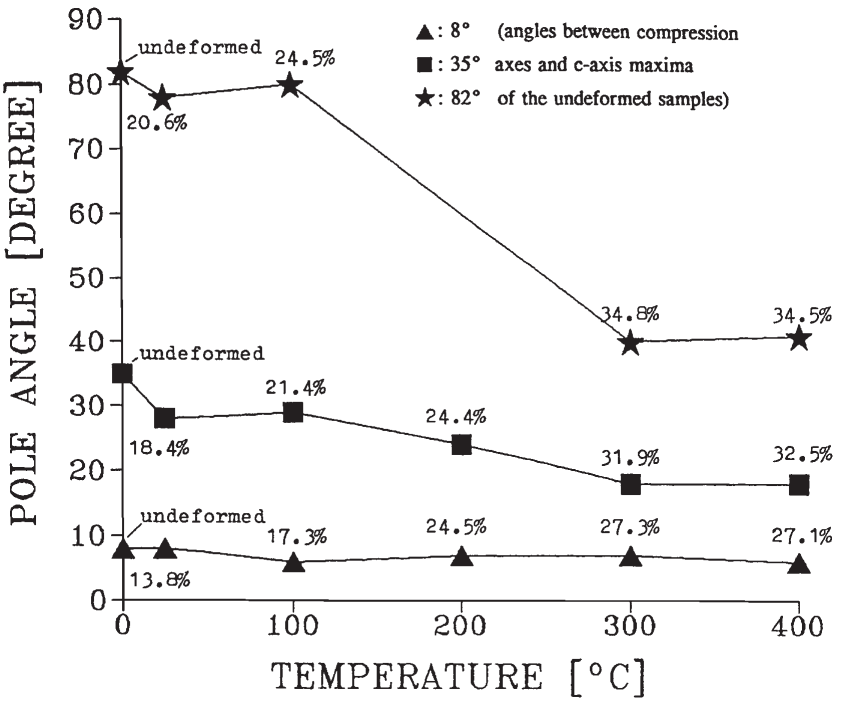

Fig. 21. Pyrrhotite ore from Sullivan. Reorientation of the c-axis maximum *vs*. temperature after experimental deformation. The total strain of the deformed samples is indicated; Niederschlag & Siemes (1996).

1996). A pyrrhotite ore (mainly hexagonal) from Sullivan mine, Canada, has an initial texture with a distinct c-axis maximum perpendicular to the foliation, whereas an ore (mainly monoclinic, but hexagonal at elevated temperature) from Cerro de Pasco, Peru, shows a weak and inhomogeneous texture. The samples, encapsulated in aluminium jackets, were deformed by axial compression.

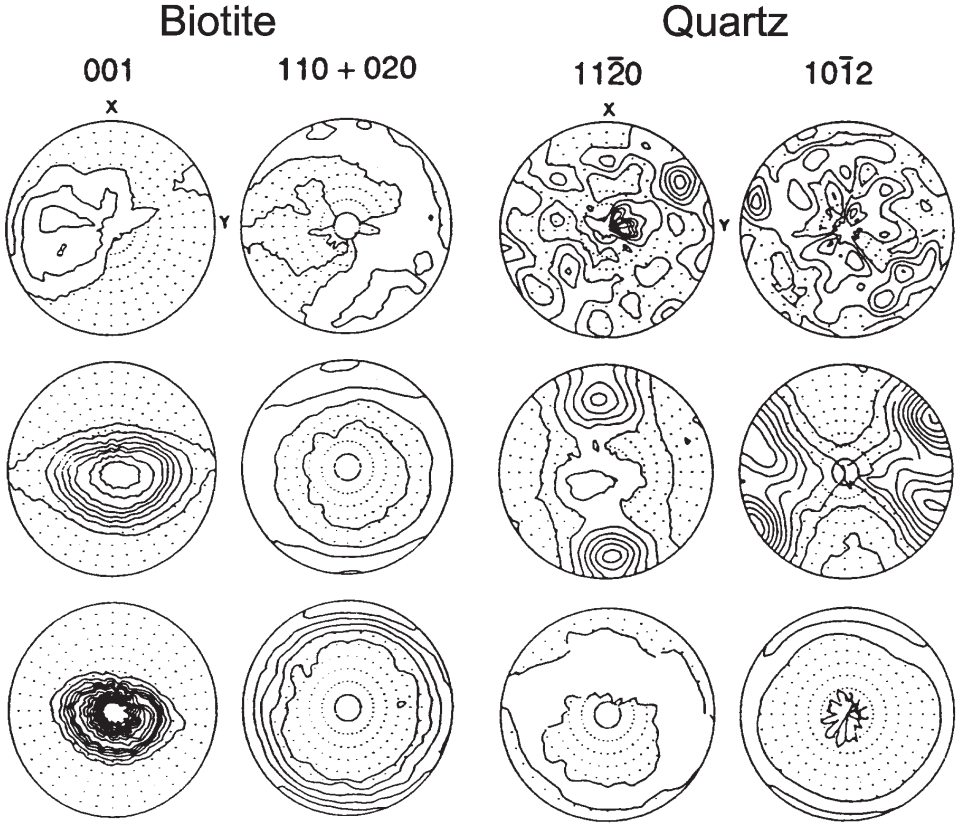

Fig. 22. Pole figures of biotite (a mica mineral) and quartz in granite from the Santa Rosa mylonite zone in Southern California, almost random distribution (top row), progressively deformed to mylonite (centre) and phyllonite (bottom row). Equal area projection; Kocks *et al.* (1998) p. 261.

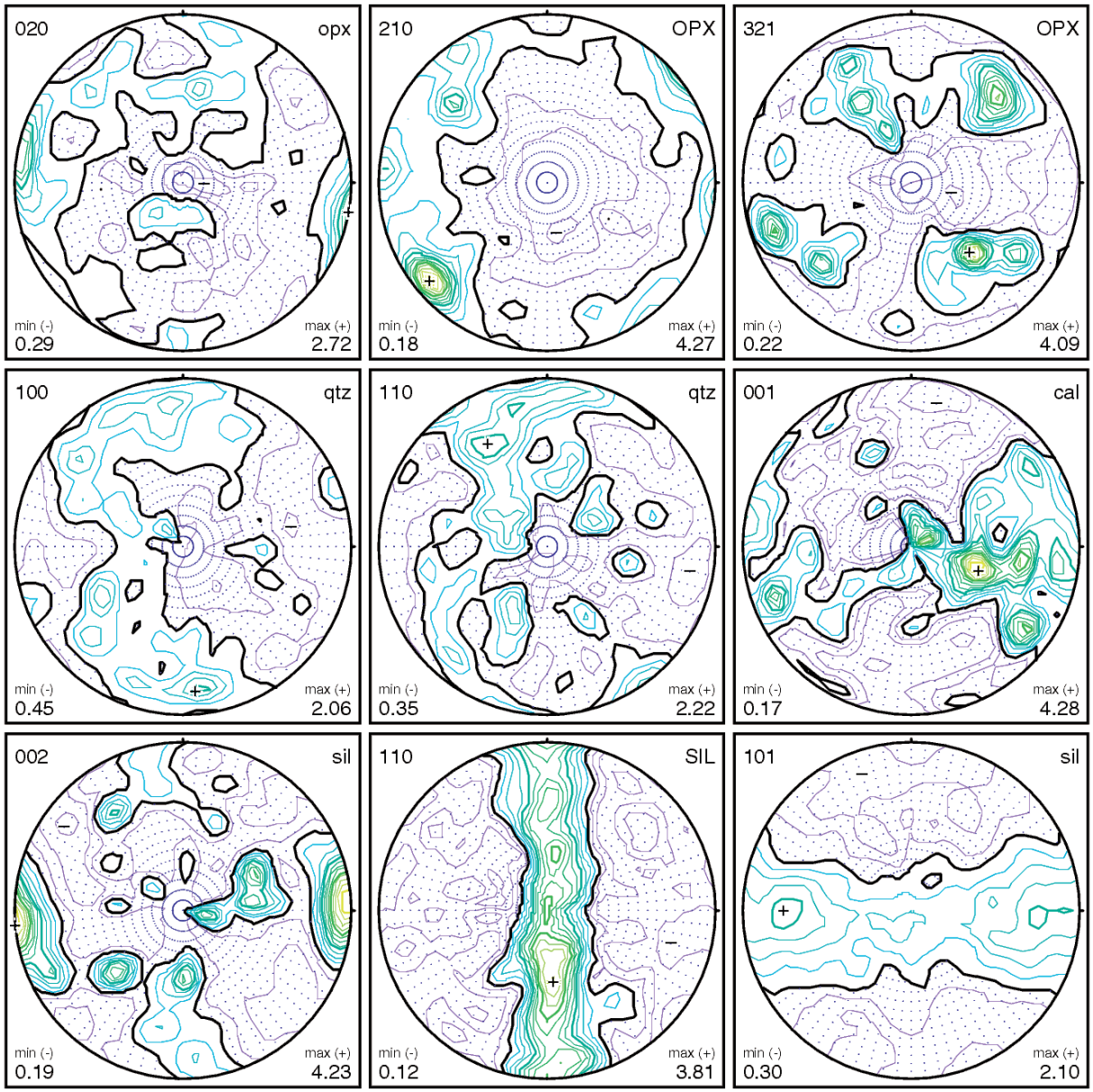

Fig. 23. Selection of separated pole figures of the mineral components bronzite (top), quartz (centre), and sillimanite (bottom) of a coarse-grained granulite rock; Gastreich *et al.* (2000).

The tests with the samples from Sullivan were performed with a constant strain rate of about $3 \cdot 10^{-5}$ s^{-1} and temperatures of 25 to 400°C and different angles (8°, 35°, 82°) between the compression axis and the initial c-axis maximum. Samples compressed at angles of 8° and 35° show a progressive tendency of the c axes to orient parallel to the compression axis. Samples compressed with an angle of 82° show the development of an a-axis maximum parallel to the compression axis. The plot of the angle between the c-axis maxima and the centres of the pole figures (Fig. 21) show the continuing reorientation of (0001) perpendicular to the compression axis with increasing temperature and total strain. The deformation textures show the influence of different activated glide modes as a function of the compression direction and temperature.

After deformation under different conditions, the Cerro de Pasco samples show a tendency of (0001) to orient perpendicularly to the compression axis while the $(11\bar{2}0)$ poles concentrate on great circles along the primitive circle. This is analogous to the texture development of the Sullivan ore compressed with angles of 8° and 35° to the initial c-axis maximum at all investigated temperatures.

The inhomogeneous texture of the starting material did not allow to draw conclusions about the texture development as a function of strain rate and temperature.

The results show that most deformation conditions (except temperatures below 200°C) lead to the reorientation of (0001) perpendicular to the compression axis or at least a strong tendency for this development. Therefore, under most conditions in the earth's crust a similar texture devel-

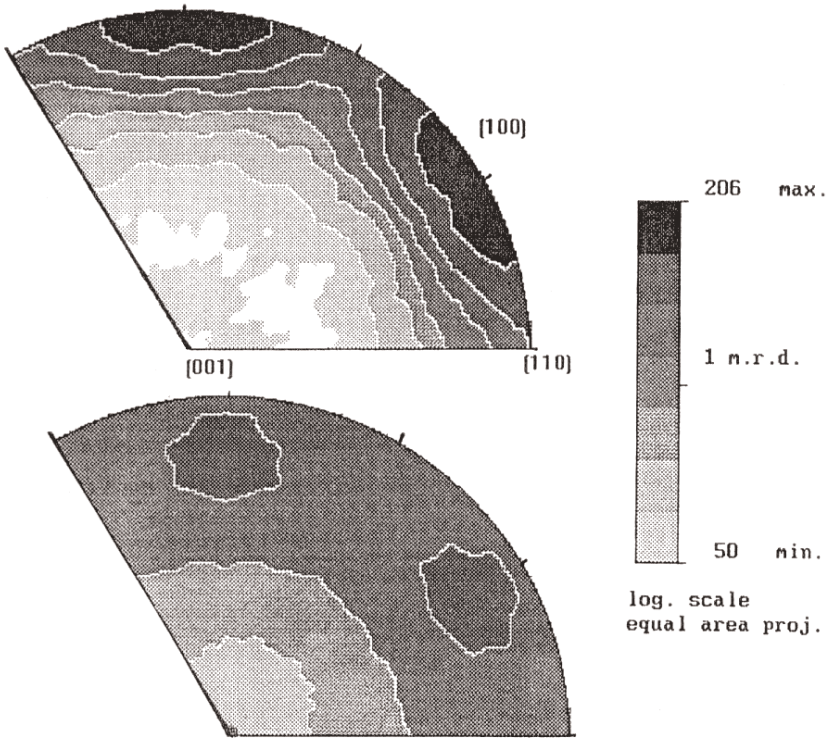

Fig. 24. Inverse pole figures of ice-II from uniaxial compression. (a) deformed 57 % and (b) deformed 7 %. Contouring interval is log scale. Axes of compression align parallel to (100); Bennett *et al.* (1994).

opment should be expected. This agrees with natural occurring textures because the texture of (0001) parallel to the foliation is very common in natural metamorphic pyrrhotite ore deposits. The study confirmed the influence of cataclastic flow at lower temperatures and decreasing strength with lower strain rate. It was shown that a strong initial texture has only little effect on the strength of pyrrhotite.

6.5 Granite

Granite rock, consisting of feldspar, quartz and mica, has been studied by neutron diffraction using a position-sensitive detector instrument (Wenk & Pannetier, 1990). Increasing deformation has been observed on the mica and quartz mineral components on different specimens originating from the Santa Rosa mylonite zone in Southern California. Figure 22 illustrates initially an almost random orientation distribution. With increasing deformation at metamorphic conditions mica and quartz experience a strong texture in mylonite and, finally, by progressive deformation to phyllonite, a further increase of the mica texture including grain-size reduction, whereas the quartz texture attenuates. According to Kocks *et al.* (1998), the texture change in quartz has been attributed to different deformation mechanisms: dislocation glide accompanied by recrystallization during the first stage, and superplastic flow during the second stage.

6.6 Orthopyroxene-Sillimanite-Granulite

A recent neutron-diffraction texture study (Gastreich *et al.*, 2000) is concerned with a granulite rock originating from the Kolivatsa-Umba Suturzone of the Kola peninsula, Russia. The main mineral components of the coarse-grained material (grains up to the mm region) are bronzite (an orthopyroxene), quartz and sillimanite. The rock's fabric is characterized by a marked foliation and lineation perpendicular to the tectonic transport direction. Pole-figure scans were performed on a cube-shaped sample of about 8 cm^3. After deconvolution of the reflection-rich diffraction patterns by profile-fitting methods a total of 17 individual pole figures (6 of bronzite, 5 of quartz and 6 of sillimanite) were obtained to evaluate the mineral textures (Fig. 23). The Mg-rich prismatic orthopyroxene (bronzite, space group *Pbca*, a = 18.16 Å, b = 8.84 Å, c = 5.19 Å) reveals a distinct orientation of the prismatic planes (210). The preferred orientation of the b axes corresponds to an east-west alignment. The formation of the texture is due to grain rotation along the lineation of the rock. The quartz texture, which was modelled by ODF calculation of the experimental pole figures, is characterized by c-axis orientations due to a prism <c>-glide mechanism, typical for high-temperature coaxial-constrictional deformation. The sillimanite phase (space group *Pbnm*, a = 7.50 Å, b = 7.74 Å, c = 5.80 Å) shows a clear directional alignment of crystallites by grain rotation analogous to the findings of the bronzite phase. The study reveals the unique potential of neutron-diffraction texture analysis on multi-phase rocks for identifying the deformation mechanisms of the different mineral phases.

6.7 Ice

Bulk-textural characterization of the interiors of moons consisting mainly of ice-rock mixtures are needed to resolve their planetary histories. Understanding the

rheology of ice at high pressure and low temperature is essential for any type of geological or geophysical interpretation of icy bodies of the outer solar system. Neutron diffraction can provide bulk-texture information on materials under special sample environments, *e.g.*, in a low-temperature cryostat. The texture of polycrystalline ice II (high-pressure polymorph of the solid form of water stable between roughly 200 and 500 MPa and below approximately 238 K, rhombohedral crystal structure) produced in low-temperature high-pressure axial-compression experiments has been investigated at 77 K (Bennett *et al.*, 1994). In two deuterated specimens (one sintered hydrostatically and shortened 50 % at 225 K, the other produced non hydrostatically and shortened 7 % at 195 K) recalculated pole figures from orientation-distribution functions (Fig. 24) show that a axes align in the direction of compression. In the low-pressure polymorph ice I deformed at low temperature, however, c axes are oriented parallel to the compression direction (Kocks *et al.*, 1998, p. 260). By measurements at the ILL it was proved that also non-deuterated ice could be measured for its texture, and ODF calculated, even with the strong incoherent scattering of H. This is of particular importance for precious ice like the one coming from deep coring expeditions.

6.8 Meteorites

The final example is not a texture investigation in its true meaning because it is concerned with fragments of single crystals rather than with polycrystalline material. Neutron-diffraction pole-figure scanning has been used to investigate rare pieces of meteorites to reveal twinning and special orientation relationships of different phases. Orientation of crystallites in meteorites occurs after phase transformation in the process of cooling or after mechanical twinning processes caused by shock events. The microstructures of three iron-nickel meteorites, two hexahedrites from Walker County, Alabama, (irregularly shaped) and Coahuila, Mexico (rectangularly shaped), and one octahedrite from Gibeon, Namibia, (cube-shaped), were analysed by performing pole-figure scans with a very narrow scanning grid involving a total of 7651 different sample orientations (Höfler *et al.*, 1988).

For both hexahedrites, pole figures of bcc-kamacite (*i.e.*, body-centred α-Fe with less than 6 wt% Ni) have been measured. Two kinds of pole-density maxima are observed differing in intensity and extension (Fig. 25). Peaks with high intensities and large extensions are attributed to the face poles of symmetry-equivalent single-crystal reflections, peaks with weak intensities and small extensions to face poles of twin reflections according to a {211} twinning. The volume percentage of twins is about 6 % and 8 % for the Walker County and Coahuila samples, respectively, as estimated from the intensity relation of monocrystal and twin intensities. While the Coahuila meteorite is characterized by rather symmetric pole-density maxima, one observes at the Walker County rather asymmetric shapes with several diffuse extensions. This has to be attributed to the existence of several small kamacite pieces with slightly different orientations due to a breakage inside the meteoritic specimen.

The octahedritic Gibeon was analysed with respect to taenite (*i.e.*, γ-Fe with about 30 wt% Ni) and kamacite orientation relationships. Taenite pole figures reveal that taenite rims have the orientation of the parent γ-phase crystal. The kamacite pole figures (Fig. 25) are characterized by groups and bands with several intensity maxima. The orientation of kamacite lamellae and taenite rims is close to the Nishiyama-Wassermann relationship ($\{110\}_\alpha \parallel \{111\}_\gamma$, $<001>_\alpha \parallel <-110>_\gamma$. Variant selection occurs with the kamacite crystals and suggests the presence of strain during kamacite growth.

7. Strain/stress in rocks

The knowledge of the strain/stress behaviour of rocks in the earth's crust is very important for the understanding of tectonic processes. Knowledge of the magnitude of differential stress provides constraints on the mechanical behaviour of rocks at depth and is a necessary prerequisite for modelling the rheology of the lithosphere. One important aspect is earthquake research which increasingly requires an improvement in data quality both for modelling tests of the deformation behaviour of single crustal structures and for studies of regional hazard assessment (Frischbutter, 1998). Palaeopiezometry is a traditional method of stress measurement in geosciences which can be applied to rocks deformed by dislocation creep. Comparative studies of neutron diffraction and palaeopiezometry on deformed rocks are promising applications of neutron diffraction in geosciences (Kenkmann, 1999). Up to now, however, intracrystalline strain measurements on geological samples by diffraction experiments were not used. In contrast to this, neutron diffraction has been a well-established technique for many years to measure macrostrain in materials like metals, alloys, and corresponding industrial and technological components (*e.g.*, rails or turbine blades) due to the capability of neutrons to "look" into the volume interior.

The levels of intracrystalline lattice strain are quite different in technological and geological materials as has been discussed by Pintschovius *et al.* (2000). Residual or load strains in metals are typically of the order 10^{-3} and in ceramic materials only a few times 10^{-4}. Hence, a precision as high as 2×10^{-5} is needed and has been achieved using high-resolution neutron diffractometers. However, many geological samples are expected to show even lower levels of residual strain because drilling gives rise to stress relaxation which will wipe out the macrostresses when a sample is brought to the surface. A sample located in a tectonically inactive region implying low shear stresses, and drilled from a depth of about 250 m will show residual strains only of the order 10^{-5}. Thus, an accuracy of about 10^{-6} is necessary to obtain reliable diffraction results.

The situation, however, becomes more favourable in case of *in situ* experiments without any disturbances of the stress state by drilling. Here, high-resolution neutron diffraction under defined conditions of pressure and

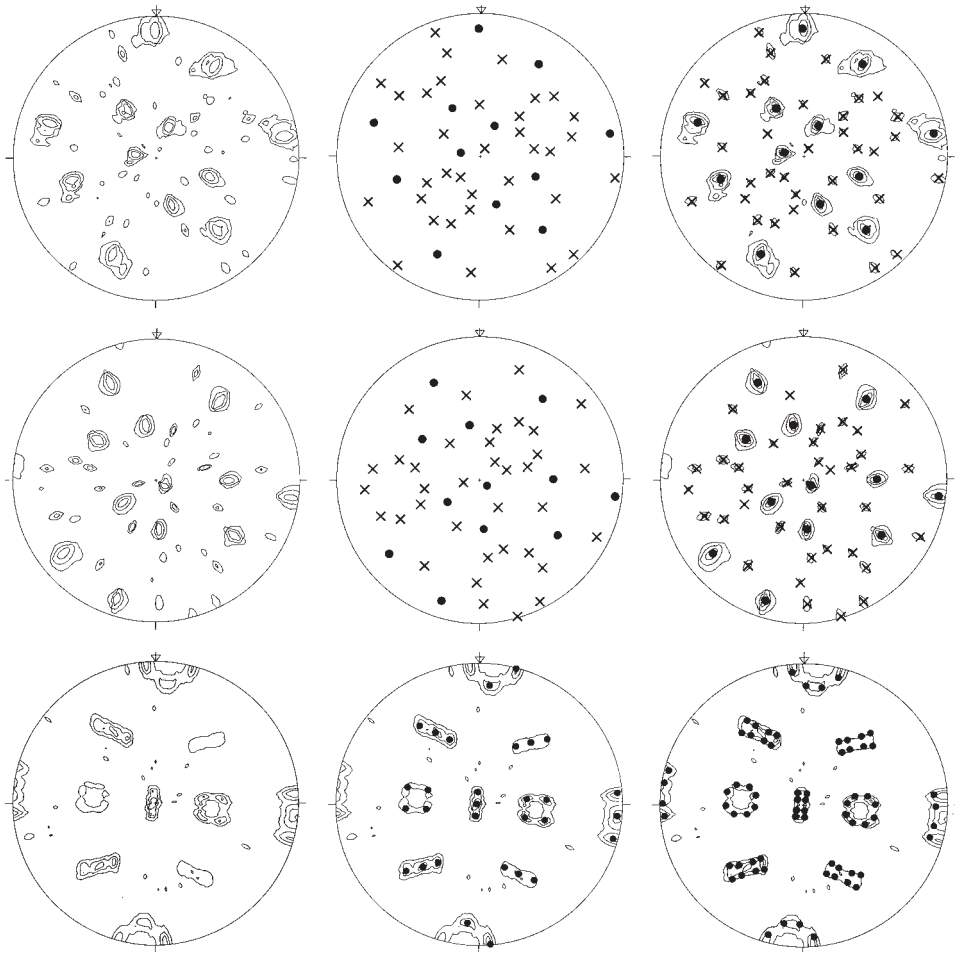

Fig. 25. 211 pole figures of Walker County (top row) and Coahuila (central row) and 200 kamacite pole figures of Gibeon (bottom row); Höfler *et al.* (1988).

temperature can provide useful information, *e.g.*, on strain/stress differences in different rock minerals.

8. Strain/stress analysis by diffraction methods

Strain analysis by diffraction methods refers to measurements of both macroscopic lattice deformation (first order strain ε) and of microscopic crystallite deformation (second and third order strain ε′) resulting in peak shifts and peak broadenings, respectively. Microstrain broadening is often superimposed by particle-size broadening, *i.e.*, grain-size reduction limiting the coherently scattering sample volume. The differentiation between size and microstrain broadening is performed by peak-profile analysis indicating Lorentzian and Gaussian forms of peak broadening, respectively (*e.g.*, de Keijser *et al.*, 1983). A useful and quick assessment of line broadening by either microstrain or grain-size effect is performed by the Williams-Hall plot (Williamson & Hall, 1953) according to

$$\mathrm{FWHM} \cdot \cos\Theta = \lambda / b + C \cdot \varepsilon' \cdot \sin\Theta \qquad (11)$$

where the product of the integral line breadth (FWHM · cos Θ) is plotted versus sin Θ for the determination of the size parameter b and the microstrain parameter ε′; C is a constant.

Macroscopic strain ε, however, is analysed by 2Θ-peak shifts caused by changes of d-spacings inside the macroscopically deformed material, according to Bragg's law given by equation (4). Thus, atomic lattice planes are used as an atomic «strain gauge». Accordingly, the relative strain ε is expressed by

$$\varepsilon = (d - d_0) / d_0 \qquad (12)$$

where d_0 denotes d-spacings of the undeformed material. During the diffraction experiment a selected volume element of the sample, which is defined in its size and position by diaphragms installed in the incident and diffracted neutron beam before and behind the sample, respectively, is scanned with respect to the sample-fixed coordinate system (x, y, z) by using the (φ, χ)-rotations of a Eulerian cradle for different scattering vector orientations (see Fig. 3). The experiment provides the orientation dependent strain components ($\psi = 90° - \chi$)

$$\varepsilon_{\varphi\psi} = (d_{\varphi\psi} - d_0) / d_0 \qquad (13).$$

The strain is represented by six components ε_{ij} of a second-rank tensor. According to Noyan (1991), the fundamental

equation for strain/stress analysis with diffraction is

$$(d_{\varphi\psi} - d_0) / d_0 = \varepsilon_{11}\cdot\cos^2\varphi\cdot\sin^2\psi + \varepsilon_{12}\cdot\sin^2\varphi\cdot\sin^2\psi + \varepsilon_{22}\cdot\sin^2\varphi\cdot\sin^2\psi + \varepsilon_{33}\cdot\sin^2\psi - \varepsilon_{33} + \varepsilon_{13}\cdot\cos\varphi\cdot\sin^2\psi + \varepsilon_{23}\cdot\sin\varphi\cdot\sin^2\psi \quad (14).$$

Measurements of at least six different orientations are necessary to solve this system of linear equations for the determination of $d_{\varphi\psi}$.

Hooke's law,

$$\sigma = E \cdot \varepsilon \quad (15)$$

containing the elasticity term E, is used to calculate the sample characterizing stress σ. The stress field is described by a symmetrical tensor of nine components σ_{ij}, six of which are independent because of the symmetry condition $\sigma_{ij} = \sigma_{ji}$.

9. Neutron strain diffractometers

Analogous to texture diffractometers (see chapter 4) neutron strain diffractometers are operated at both continuous and pulsed beam sources. Strain experiments at reactor sources are performed on two-axis powder diffractometers which, in general, are equipped with large position-sensitive detectors and special sample environments like Eulerian cradle, x,y,z-translation devices and primary and secondary diaphragms of adjustable geometry before and behind the sample, respectively. Such instruments are, for example, E3 at the BER-II reactor of the Hahn-Meitner-Institute in Berlin and also the high-intensity and variable-resolution diffractometer D20 at ILL. So far, however, these instruments are in routine use for residual stress analysis only in applied materials science, where the requirements in physical Δd/d resolution are less pronounced compared to the demands for geomaterials.

Better resolution can be obtained with pulsed sources taking advantage of the potential of time-of-flight technique. The dedicated strain/stress neutron diffractometer EPSILON has been built at the pulsed reactor IBR-2 in Dubna (Walther *et al.*, 1998, 1999). The total neutron flight path from the moderator to the detector is almost 103 m. Actually, EPSILON operates with four detectors (Fig. 26), where a couple of detectors are positioned on each side at Bragg angles 2Θ = 90°. This geometry allows the simultaneous measurement in two directions defined by two scattering vectors oriented perpendicular to each other (compare Fig. 26). The instrument is equipped with the special pressure device EXSTRESS for compressive uniaxial load. The maximum force is 100 kN, *i.e.*, 150 MPa for cylindrical sample dimensions of 30 mm diameter and 60 mm length (see chapter 10.1). An envisaged improved detector installation will allow the measurement of the peak shift in nine variant directions and will therefore allow the estimation of the full stress tensor without any sample rotations (compare chapter 4.2.4.).

ENGIN is the dedicated strain scanning time-of-flight instrument at the ISIS spallation source. Its characteristics

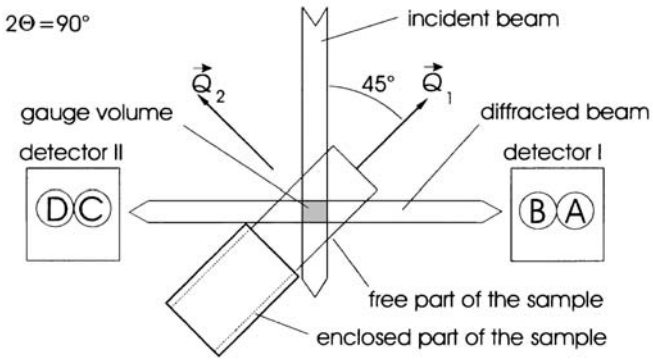

Fig. 26. Measurement geometry of the neutron strain TOF diffractometer EPSILON with four detectors A, B, C, D and scattering vectors Q_1 and Q_2 (Scheffzük *et al.*, 1998).

are ± 90° detector banks, radial collimation and a d-spacing coverage from 0.4 Å to 3.3 Å. Actually, the Δd/d-resolution is about 0.7 % based on a neutron flight path of about 15 m and resulting in an uncertainty in lattice parameter of about $5 \cdot 10^{-5}$. Gauge dimensions are 0.5 to 25 mm incident beam in both dimensions and 1.5 mm outgoing beam fixed. An uniaxial loading rig of ± 50 kN dynamic loading can be mounted on the positioning table. Though this instrument is a dedicated engineering science facility it has recently been used also successfully for polymineralic rocks (see chapter 10.2). The application criteria with respect to geomaterials will be significantly enhanced with respect to improved Δd/d-resolution and to strain accuracy at the new beam line ENGIN-X which is currently under construction with a neutron flight path of 50 m.

10. Examples of mineral strain/stress analyses by neutrons

10.1 Full strain/stress tensor in sandstone

The EXSTRESS apparatus at the EPSILON instrument has been tested on a cylinder of Cretaceous sandstone (quartz) which was pressed into a steel tube 20 h after extraction, thus allowing the investigation of a deformed and a relaxed part on the same sample (Scheffzük *et al.*, 1998). The outstanding spectral resolution achieved for quartz gives the required precision for the estimation of the peak position. Two different strain/stress states could be distinguished in the same specimen. Within two mutually perpendicular radial directions of the cylinder, the lattice spacings are distinctly smaller within the encapsulated volume than in the free volume. Figure 27 summarizes the experimental results for both volumes by indicating the positive and negative strain rates due to stretching and compression, respectively, in three orthogonal directions. The determined strain rates are of the order 10^{-4}. Although the results cannot be finally interpreted yet, the influence and importance of texture in strain/stress behaviour of rocks becomes obvious.

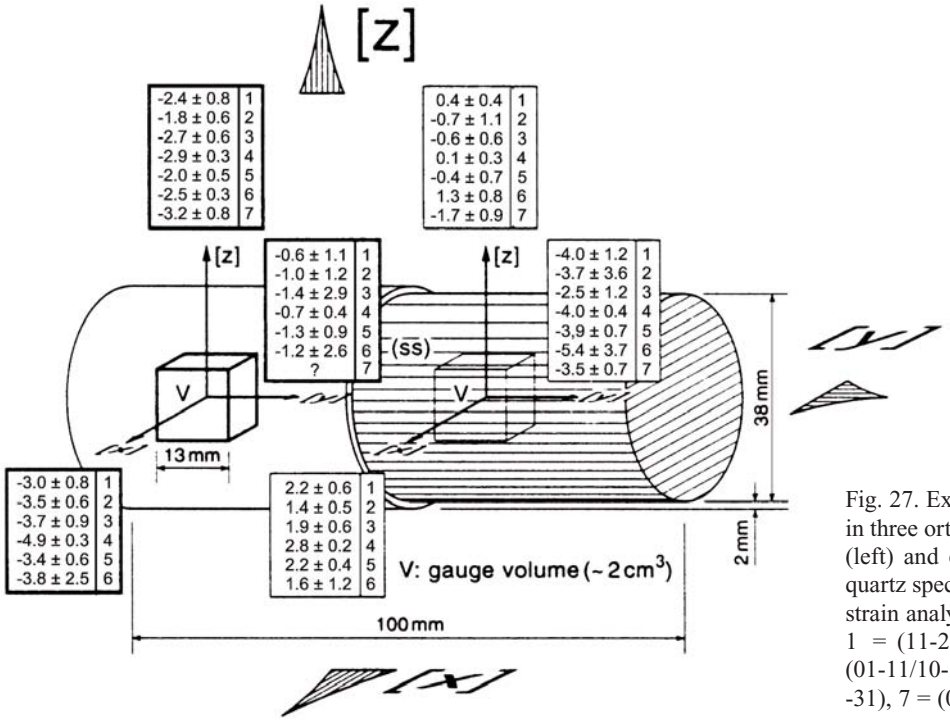

Fig. 27. Experimental strain rates ε in units of 10^{-4} in three orthogonal directions x, y and z of the free (left) and encapsulated volumes V (right) of the quartz specimen. The basic reflections used for the strain analysis are indicated by numbers behind ε: 1 = (11-20), 2 = (11-22), 3 = (11-21), 4 = (01-11/10-11), 5 = (01-12/10-12), 6 = (12-31/21-31), 7 = (02-21/20-21) (Scheffzük *et al.*, 1998).

10.2 Strain partitioning in polymineralic rocks

The understanding and interpretation of seismological data is heavily reliant upon the knowledge of the elastic properties of the relevant rock types. For the first time, neutron-diffraction strain measurements open the possibility to study the elastic properties of the individual components of polymineralic materials and to establish the relative contribution of each phase to the rock's properties. The strain partitioning between the component phases in olivine + magnesiowüstite (Covey-Crump *et al.*, submitted) and in calcite + halite aggregates (Rinaldi *et al.*, 2001) has been analysed from *in situ* rock-deformation experiments where the sample was held under different loads in the neutron beam using the ENGIN facility at ISIS. By determining the changes in lattice parameters of each component phase as a function of applied load, the elastic strain of each phase, and hence its contribution to the total deformation, has been ascertained (see Fig. 28). The calcite/halite measurements revealed that the elastic limit of the halite was at a halite strain of about 350 μstrain and that the elastic strain partitioning between the two phases was unaffected by the yielding of the halite. Above a calcite elastic strain of about 550 μstrain the strain partitioning between the two phases started to tend towards homogeneous elastic strain. The curve describing the elastic strain partitioning was independent of composition.

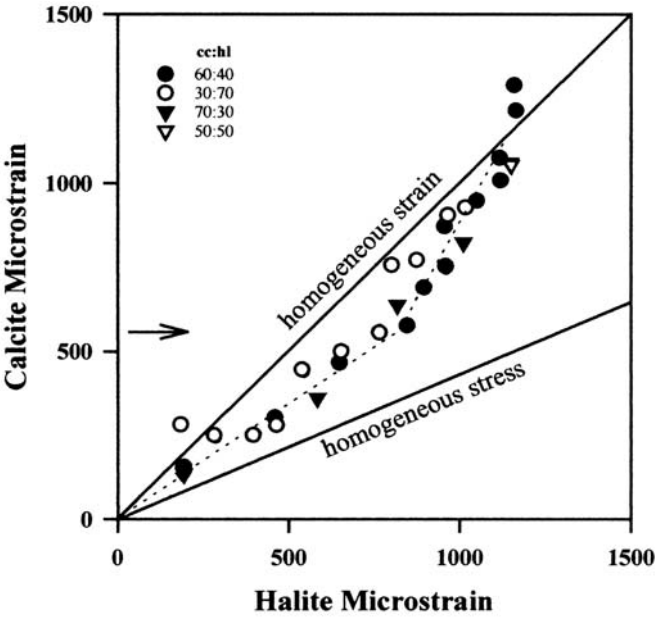

Fig. 28. Calcite and halite axial elastic strains at different applied loads. Also shown are the predicted phase strains assuming homogeneous strain and homogeneous stress. The dashed line shows the trend in the data (calcite ≥ 50 %) and the arrow shows the calcite strain at the elastic limit (Rinaldi *et al.*, 2001).

11. Conclusions and prospects

In the last decade, neutron diffraction has opened a new dimension and new quality in quantitative texture analysis of minerals and geomaterials. The progress is based (a) on the high penetration capability of neutrons, (b) on the large size of neutron beams, and (c) on the instrumental and methodical progresses in pole-figure preparation. The main advantages of neutrons when analysing geomaterials are

(1) high grain statistics (millions of grains versus hundreds of grains as analysed by U-stage microscopy), (2) the investigation of global-volume textures rather than local (surface) textures by X-ray diffraction, (3) studies on both fine- and coarse-grained natural materials, (4) texture analyses of low-symmetry minerals, and (5) investigations on multi-phase rocks allowing texture analyses of the individual mineral components.

Quantitative ODF analyses using neutrons are already now accessible to polyphasic geological materials as has been demonstrated *e.g.*, on a rock composed of quartz, biotite and feldspar by Chateigner *et al.* (1999). The application of a new Rietveld technique combined to ODF calculation will be the method of choice in polycrystalline diffraction-data evaluation. The main challenges are to obtain the orientation distribution in the case of low-symmetry compounds and to analyse the crystal structure in the presence of strong texture. Several efforts have been undertaken and studies are well on their way to perform a combined structure, texture and strain/stress analysis.

Wenk *et al.* (1994) proposed a method which uses the whole diffraction spectrum rather than extracted peak intensities, by combining ODF calculation with the crystallographic Rietveld method. The method is particularly elegant using TOF neutron-diffraction saving beam time by using small pole-figure regions and many diffraction lines. The feasibility of the RiTA-method (Rietveld texture analysis) has been illustrated with neutron TOF data of experimentally deformed calcite. It was possible to obtain quantitative information on texture, crystal structure, microstructure and residual stress from highly incomplete pole figures and from regions of the diffraction spectrum containing many overlapping peaks (Lutterotti *et al.*, 1997).

Von Dreele (1997) has implemented a generalized spherical-harmonic description of the texture in a multiple-phase/multiple-data-set Rietveld refinement code. It has been tested using two sets of neutron time-of-flight data taken from the standard calcite sample previously used for the round-robin study (compare chapter 6.1 and Wenk, 1991). Texture results obtained are similar to those from individual pole figures. However, programs such as the user-friendly MAUD program (Lutterotti *et al.*, 1999) have not yet been applied to complex geological materials.

It should be stated, however, that, so far, the knowledge of the potential of neutron diffraction in geological texture analysis is not widespread in the community of geoscientists. One reason is the limited number of neutron instruments and restrictions with respect to measuring times especially when large suites of samples have to be analysed, despite the increased efficiencies of neutron instruments in recent years. Further efforts are necessary to transfer and extend the know-how, acquired by crystallographers and materials scientists over many years in the field of quantitative texture and strain/stress analysis, to standard applications in geoscience.

Future prospects of combined neutron diffraction texture and strain/stress analysis on geomaterials are encouraging, especially when looking at advanced pulsed spallation sources. In particular diffraction can profit from increased neutron peak flux and instrumental resolution by time-of-flight techniques. Prospects are excellent with regard to the potential of the envisaged European Spallation Source (ESS). In the field of mineral and earth sciences, the advisory science board of ESS has defined a flagship experiment for the investigation of stress and texture development upon deforming geomaterials (Richter, 2001). The two experiments should be performed simultaneously, in order to follow the complete evolution of the sample under real high-temperature and high-pressure conditions to simulate large-scale deformation of crustal and mantle materials. Neutron diffraction has the potential to investigate the development of microstructures involving twinning, phase transitions, mineral structural and textural transformations and strain/stress formation simultaneously using only one single instrument.

References

Bennett, K., Wenk, H.-R., Choi, C.S., Trevino, S.F., Durham, W.B., Stern, L.A. (1994): Texture measurement at 77 K of deformed D_2O ice II polycrystals: a study by neutron diffraction. *in* "Textures of Geological materials", H.J. Bunge, S. Siegesmund, W. Skrotzki, K. Weber, Eds. DGM Informationsgesellschaft, Oberursel, 251-260.

Bennett, K., von Dreele, R.B., Wenk, H.-R. (1999): "HIPPO", a new high intensity neutron diffractometer for characterization of bulk materials. *in* "Proc. ICOTOM-12", J.A. Szpunar, Ed. NRC Research Press, Ottawa, Canada. Vol. 1, 129-134.

Brokmeier, H.-G. (1994): Application of neutron diffraction to measure preferred orientations of geological materials. *in* "Textures of Geological Materials" . H.J. Bunge, S. Siegesmund, W. Skrotzki, K. Weber Eds. DGM Informationsgesellschaft, Oberursel, 327-344.

Brokmeier, H.-G., Zink, U., Schnieber, R., Witassek, B. (1998): TEX-2, Texture Analysis at GKSS Research Center. *Mat. Sci. Forum*, **273-275**, 277-282.

Bunge, H.J. (Ed.) (1982): "Texture Analysis in Materials Science, Mathematical Methods". Butterworths & Co. Publishers, London, 593 p.

– (1986): Quantitative Texture Analysis. DGM Informationsgesellschaft, Oberursel.

Bunge, H.J. (1997): X-ray texture analysis in materials and earth sciences. *Eur. J. Mineral.*, **9**, 735-761.

Bunge, H.J., Wenk, H.-R., Pannetier, J. (1982): Neutron diffraction texture analysis using a 2Θ-position sensitive detector. *Textures and Microstructures*, **5**, 153-170.

Bunge, H.J., Siegesmund, S., Skrotzki, W., Weber, K. (Eds.) (1994): "Textures of Geological Materials". DGM Informationsgesellschaft, Oberursel. 399 p.

Caglioti, G., Paoletti, A., Ricci, F.P. (1958): On resolution and luminosity of a neutron powder spectrometer. *Nucl. Intrum. Methods*, **3**, 223-228.

Chateigner, D., Wenk, H.-R., Pernet, M. (1999): Orientation distributions of low symmetry polyphase materials using neutron diffraction data: Application to a rock composed of quartz, biotite and feldspar. *Textures and Microstructures*, **33**, 35-43.

Dahms, M. & Bunge, H.J. (1989): The iterative series-expansion method for quantitative texture analysis. I. Gerneral outline. *J. Appl. Cryst*., **22**, 439-447.

Elf, F., Schäfer, W., Höfler, S., Will, G. (1990): Texture investigations at low temperatures by neutron diffraction shown on the example of TbAg. *Textures and Microstructures*, **13**, 55-58.

Feldmann, K., Betzl, M., Andreeff, A., Hennig, K., Kleinstück, K., Matz, W. (1980): Comparison of quantitative texture analysis results from time-of-flight and conventional neutron diffraction. *Texture of Crystalline Solids*, **4**, 1-11.

Feldmann, K., Betzl, M., Kleinsteuber, W., Walther, K. (1991): Neutron time-of-flight texture Analysis. *Textures and Microstructures*, **14-18**, 59-64.

Frischbutter, A. (1998): Intrakristalline Strainmessung mit Neutronenbeugungsmethoden, Schriftenreihe für Geowissenschaften 6. A. Frischbutter Ed., Verlag der Gesellschaft für Geowissenschaften, Berlin, 7-8.

Gastreich, M., Jansen, E., Raith, M., Kirfel, A. (2000): Polfigurmessungen mit Neutronen an einem Orthopyroxen-Sillimanit-Granulit. *Z. Krist. (Suppl.)*, **No 17**, 73.

Ghildiyal, H., Jansen, E., Kirfel, A. (1999): Volume texture of a deformed quartzite observed with U-stage and neutron diffractometry. *Textures and Microstructures*, **31**, 239-248.

Helming, K. (Ed.) (1996): Texturapproximation durch Modellkomponenten, Cuvieller Verlag, Göttingen, 119 p.

Helming, K. & Eschner, T. (1990): A new approach to texture analysis of multiphase materials using a texture component model. *Cryst. Res. Technol*., **25**, K-203-K208.

Helming, K., Matthies, S., Vinel, G.W. (1988): ODF representation by means of σ-sections. *In* Proc. ICOTOM-8. Eds. J. Kallend, G. Gottstein. Warrendale. 55-60.

Helming, K., Wenk, H.-R., Choi, C.S., Schäfer, W. (1994): Description of quartz textures by components. Examples from metamorphic rocks. *in* "Textures of Geological Materials". H.J. Bunge, S. Siegesmund, W. Skrotzki, K. Weber, Eds. DGM Informationsgesellschaft, Oberursel, 303-325.

Höfler, S., Schäfer, W., Will, G. (1986): Texture measurements at the neutron diffractometer in Jülich. *in* "Experimental Techniques of Texture Analysis". H.J. Bunge, Ed.. DGM Informationsgesellschaft, Oberursel, 241-251.

Höfler, S., Will, G., Hamm, H.-M. (1988): Neutron diffraction pole figure measurements on iron meteorites. *Earth Planet. Sci. Lett.*, **90**, 1-10.

Ivankina, T.I., Nikitin, A.N., Sobolev, G.A., Sukhoparov, V.A., Telepnev, A.S., Ullemeyer, K., Walther, K. (1999): Influence of temperature and long-time loading on texture and physical property variations of a calcite marble. Intern. Conf. on Textures and Physical Properties of Rocks, Göttingen, 13.-16.10.1999.

Jansen, E., Schäfer, W., Will, G. (1986): Application of profile analysis methods in texture measurements using position-sensitive detectors. *in* "Experimental Techniques of Texture Analysis". H.J. Bunge Ed. DGM Informationsgesellschaft, Oberursel, 229-240.

– , – , – (1988): Profile fitting and the two-stage method in neutron powder diffractometry for structure and texture analysis. *J. Appl. Cryst*., **21**, 228-239.

Jansen, E.M., Merz, P., Schaeben, H., Schäfer, W., Siemes, H., Will, G. (1992): Determination of preferred orientation of pyrite in a chalcopyrite ore by means of neutron diffraction. *Textures and Microstructures*, **19**, 203-210.

Jansen, E.M., Siemes, H., Merz, P., Schäfer, W., Will, G., Dahms, M. (1993): Preferred orientation of experimentally deformed Mt Isa chalcopyrite ore. *Min. Mag.*, **57**, 45-53.

Jansen, E., Schäfer, W., Kockelmann, W., Will, G. (1996a): Multiple pole figure extraction from pulsed white beam angle-dispersive neutron diffraction data. *Textures and Microstructures*, **26-27**, 11-18.

Jansen, E., Schäfer, W., Will, G., Knight, K.S. (1996b): Neutron diffraction pole figure measurements using a pulsed white beam and the linear JULIOS-detector. *Materials Science Forum*, **228-231**, 259-264.

Jansen, E., Schäfer, W., Skowronek, R., Kirfel, A., Höpfer, N., Ghildiyal, H., Siemes, H., Klingenberg, B., Rybacki, E. (1999): Volumentexturen hoch- und niedersymmetrischer geologischer Proben – Ergebnisse vom Verbund-Texturdiffraktometer SV7b in Jülich. Deutsche Neutronenstreutagung n99, Potsdam, 25-27.05.1999.

Jansen, E., Schäfer, W., Kirfel, A. (2000a): The Jülich neutron diffractometer and data processing in rock texture investigations. *J. Struct. Geol.*, **22**, 1559-1564.

Jansen, E., Bauer, W., Schäfer, W. (2000b): Neutron diffraction pole figures of geological anorthosite textures. Proc. ECNS'99. *Physica B*, **276-278**, 948-949 .

Jensen, D.J. (1986): Fast texture measurement by neutron diffraction using a linear position-sensitive detector. *in* "Experimental Techniques of Texture Analysis". H.J. Bunge Ed. DGM Informationsgesselschaft, Oberursel, 217-228.

– (1992): Kinetic texture measurements. *Neutron News*, **3**, 20-23.

Jensen, D.J. & Kjems, J.K. (1983): Apparatus for dynamical texture measurements by neutron diffraction using a position sensitive detector. *Textures and Microstructures*, **5**, 239-251.

de Keijser, Th. H., Mittemeijer, E.J., Rozendaal, H.C.F. (1983): The determination of crystallite-size and lattice strain parameters in conjunction with the profile refinement method for the determination of crystal structures. *J. Appl. Cryst.*, **16**, 309-316.

Kenkmann, T. (1999): Palaeopiezometry and neutron diffraction: two stimulating methods of stress determination in deformed rocks. Intern. Conf. on Textures and Physical Properties of Rocks, Göttingen, 13.-16.10.1999.

Kocks, U.F., Thomé, C.N., Wenk, H.-R. (Eds.) (1998): Texture and Anisotropy, Cambridge University Press, Cambridge, 676 p.

Leiss, B., Ullemeyer, K., Weber, K. (Eds.) (2000): Textures and Physical Properties of Rocks. Special Issue: *J. Struct. Geol.*, **22**, No. 11/12.

Lutterotti, L., Matthies, S., Wenk, H.-R., Schultz, A.S., Richardson Jr., J.W. (1997): Combined texture and structure analysis of deformed limestone from time-of-flight neutron diffraction spectra. *J. Appl. Phys*., **81**, 594-599.

Lutterotti, L., Matthies, S., Wenk, H.-R. (1999): MAUD (Material Analysis Using Diffraction): A user friendly JAVA program for Rietveld texture analysis and more. *in* "Proc. ICOTOM-12". J.A. Szpunar Ed. NRC Research Press, Ottawa, Canada. Vol. 1, 599-1604.

Matthies, S. (1979): On the reproducibility of the orientation distribution function of texture samples from pole figures (ghost phenomena). *Phys. Stat. Sol. (b)*, **92**, K135-K138.

Matthies, S., Wenk, H.-R., Vinel, G.W. (1988): Some basics concepts of texture analysis and comparison of three methods to calculate orientation distributions from pole figures. *J. Appl. Cryst*., **21**, 285-304.

Merz, P., Jansen, E., Schäfer, W., Will, G. (1990): PROFAN-PC: a PC program for powder peak profile analysis. *J. Appl. Cryst*., **23**, 444-445.

Niederschlag, E. & Siemes, H. (1996): Influence of initial texture, temperature and total strain on the texture development of polycrystalline pyrrhotite ores in deformation experiments. *Textures and Microstructures*, **28**, 129-148.

Noyan, I.C. (1991): The theory of stress/strain analysis with diffraction. *in* "NATO ASI series; Series E, Applied sciences". Hutchinmgs, M.T. & Krawitz, A.D., Eds. Kluwer Academic Publishers, No. 216, pp 51-65.

Pintschovius, L., Prem, M., Frischbutter, A. (2000): High precision neutron diffraction measurements for the determination of low-

level residual stresses in a sandstone. *in* "Textures and Physical Properties of Rocks". B. Leiss, K. Ullemeyer, K. Weber, Eds. *J. Struct. Geol.*, **22**, 1581-1585.

Richter, D. (Ed.) (2001): Scientific Trends in Condensed Matter Research and Instrumentation Opportunities at ESS. Workshop held at Engelberg (CH), May 3-5 (2001). Progress Report ESS/SAC/Report 1/01, Forschungszentrum Jülich.

Rietveld, H.M. (1969): A profile refinement method for nuclear and magnetic structures. *J. Appl. Cryst.*, **2**, 65-71.

Rinaldi, R., Artioli, G., Dove, M.T., Schäfer, W., Schofield, P.F., Winkler, B. (2001): Neutron scattering in mineral science, earth science, and related fields with the European spallation source (ESS). *in* "Scientific Trends in Condensed Matter Research and Instrumentation Opportunities at ESS". Richter, D., Ed.; Progress Report ESS/SAC/Report 1/01, Forschungszentrum Jülich, 91-106.

Sander, B. (Ed.) (1950): Einführung in die Gefügekunde der geologischen Körper. Vol. 2. Springer, Wien, 408 p.

Schaeben, H. (1988): Entropy optimization in texture goniometry, I: Methodology. *Phys. Stat. Solidi (b)*, **148**, 63-72.

Schaeben, H. (Ed.) (1994): Diskrete mathematische Methoden zur Berechnung und Interpretation von kristallographischen Orientierungsdichten. DGM Informationsgesellschaft, Oberursel, 137 p.

Schäfer, W., Merz, P., Jansen, E., Will, G. (1991): Neutron diffraction texture analysis of multi-phase and low-symmetry materials using the position-sensitive detector JULIOS and peak deconvolution methods. *Textures and Microstructures*, **14-18**, 65-71.

Schäfer, W., Jansen, E., Merz, P., Will, G., Wenk, H.-R. (1992): Neutron diffraction texture investigation on deformed quartzites. *Physica B*, **180 & 181**, 1035-1038.

Schäfer, W., Jansen, E., Will, G. (1993): Angle-dispersive time-of-flight diffraction in a pulsed beam: an efficient technology to exploit the thermal neutron spectrum. *J. Appl. Cryst.*, **26**, 660-669.

Schäfer, W., Jansen, E., Skowronek, R., Will, G., Kockelmann, W., Schmidt, W., Tietze-Jaensch, H. (1995a): Setup and use of the ROTAX instrument at ISIS as angle-dispersive neutron powder and texture diffractometer. *Nucl. Instrum. Methods in Physics Research A*, **364**, 179-185.

Schäfer, W., Jansen, E., Will, G., Szepesvary, A., Reinartz, R., Müller, K.D. (1995b): Update on the Jülich linear and area neutron scintillation detectors. *Physica B*, **213 & 214**, 972-974.

Schäfer, W., Kockelmann, W., Jansen, E., Will, G. (1997): Comparative diffraction experiments using monochromatic and pulsed white neutrons. *Physica B*, **234-236**, 1090-1092.

Scheffzük, Ch., Frischbutter, A., Walther, K. (1998): Intracystalline strains measurements with time-of-flight neutron diffraction: Application to a Cretaceous sandstone from the Elbzone (Germany). *in* "Schriftenreihe für Geowissenschaften 6". A. Frischbutter, Ed. Verlag der Gesellschaft für Geowissenschaften, Berlin, 39-48.

Siemes, H., Zilles, D., Cox, S.F., Merz, P., Schäfer, W., Will, G., Schaeben, H., Kunze, K. (1993): Preferred orientation of experimentally deformed pyrite measured by means of neutron diffraction. *Min. Mag.*, **57**, 29-43.

Skrotzki, W. (1994): Mechanisms of texture development in rocks. *in* "Textures of Geological Materials". H.J. Bunge, S. Siegesmund, W. Skrotzki, K. Weber, Eds. DGM Informationsgesellschaft Oberursel, 167-186.

Ullemeyer, K., Helming, K., Siegesmund, S. (1994): Quantitative texture analysis of plagioclase. *in* "Textures of Geological Materials". H.J. Bunge, S. Sieesmund, W. Skrotzki, K. Weber, Eds. DGM Informationsgesellschaft, Oberursel, 93-108.

Ullemeyer, K., Spalthoff, P., Heinitz, J., Isakov, N.N., Nikitin, A.N., Weber, K. (1998): The SKAT texture diffractometer at the pulsed reactor IBR-2 at Dubna: experimental layout and first measurements. *Nucl. Instrum. Methods in Physics Research A*, **412**, 80-88.

Von Dreele, R.B. (1997): Quantitative texture analysis by Rietveld refinement. *J. Appl. Cryst*., **30**, 517-525.

Walther, K., Heinitz, J., Ullemeyer, K., Betzl, M. (1995): Time-of-flight texture analysis of limestone standard: Dubna results. *J. Appl. Cryst*., **28**, 503-507.

Walther, K., Frischbutter, A., Scheffzük, Ch. (1998): The diffractometer EPSILON for the measurement of strains: an estimation of the full stress tensor. *in* "Schriftenreihe für Geowissenschaften 6". A. Frischbutter Ed. Verlag der Gesellschaft für Geowissenschaften, Berlin, 18-28.

Walther, K., Frischbutter, A., Lieckefett, R., Scheffzük, Ch. (1999): A pressure device for strain measurements of geomaterials at the neutron diffractometer EPSILON. *in* "Proc. ICOTOM-12". J.A. Szpunar, Ed. NRC Research Press, Ottawa, Canada. Vol. 1, 1605-1609.

Wenk, H.-R. (Ed.) (1985): Preferred Orientation in Deformed Metals and Rocks: An Introduction to Modern Texture Analysis, Academic Press, New York, 610 p.

– (1991): Standard project for pole-figure determination by neutron diffraction. *J. Appl. Cryst.*, **24**, 920-927.

– (1998): Typical textures in geological materials. *in* "Textures of Geological Materials". H.J. Bunge, S. Siegesmund, W. Skrotzki, K. Weber, Eds. DGM Informationsgesellschaft, Oberursel, 240-281.

Wenk, H.-R. & Christie, J.M. (1991): Comments on the interpretation of deformation textures in rocks. *J. Struct. Geol.*, **13**, 1091-1110.

Wenk, H.-R. & Pannetier, J. (1990): Texture development in deformed granodiorites from the Santa Rosa mylonite zone, southern California. *J. Struct. Geol.*, **12**, 177-184.

Wenk, H.-R., Kern, H., Schäfer, W., Will, G. (1984): Comparison of neutron and X-ray diffraction in texture analysis of deformed carbonate rocks. *J. Struct. Geol.*, **6**, 687-692.

Wenk, H.-R., Bunge, H.J., Jansen, E., Pannetier, J. (1986): Preferred Orientation of Plagioclase – Neutron diffraction and U-stage Data. *Tectonophysics*, **126**, 271-284.

Wenk, H.-R., Larson, A.C., Vergamini, Ph.H., Schultz, A.J. (1991): Time-of-flight measurements of pulsed neutrons and 2d detectors for texture analysis of deformed polycrystals. *J. Appl. Phys.*, **70**, 2035-2040.

Wenk, H.-R., Matthies, S., Lutterotti, L. (1994): Texture analysis from diffraction spectra. *Materials Science Forum*, **157-162**, 473-480.

Will, G., Schäfer, W., Merz, P. (1989): Texture analysis by neutron diffraction using a linear position sensitive detector. *Textures and Microstructures*, **10**, 375-387.

Will, G., Merz, P., Schäfer, W., Dahms, M. (1990): Application of position sensitive detectors for neutron diffraction texture analysis of hematite ore. *Advances in X-Ray Analysis*, **33**, 277-283.

Williamson, G.K., Hall, W.H. (1953): X-ray line broadening from filed aluminium and wolfram. *Acta Metall.*, **1**, 22-31.

Received 26 September 2000
Modified version received 20 July 2001
Accepted 3 October 2001